
ROOT: Rethinking Offline Optimization as Distributional Translation via Probabilistic Bridge

Manh Cuong Dao*
 National University of Singapore
 cuongdao@nus.edu.sg

The Hung Tran*
 Washington State University
 hung.t.tran@wsu.edu

Phi Le Nguyen
 Hanoi University of Science and Technology
 lenp@soict.hust.edu.vn

Thao Nguyen Truong
 National Institute of Advanced Industrial Science and Technology
 nguyen.truong@aist.go.jp

Trong Nghia Hoang[†]
 Washington State University
 trongnghia.hoang@wsu.edu

Abstract

This paper studies the black-box optimization task which aims to find the maxima of a black-box function using a static set of its observed input-output pairs. This is often achieved via learning and optimizing a surrogate function with that offline data. Alternatively, it can also be framed as an inverse modeling task that maps a desired performance to potential input candidates that achieve it. Both approaches are constrained by the limited amount of offline data. To mitigate this limitation, we introduce a new perspective that casts offline optimization as a distributional translation task. This is formulated as learning a probabilistic bridge transforming an implicit distribution of low-value inputs (i.e., offline data) into another distribution of high-value inputs (i.e., solution candidates). Such probabilistic bridge can be learned using low- and high-value inputs sampled from synthetic functions that resemble the target function. These synthetic functions are constructed as the mean posterior of multiple Gaussian processes fitted with different parameterizations on the offline data, alleviating the data bottleneck. The proposed approach is evaluated on an extensive benchmark comprising most recent methods, demonstrating significant improvement and establishing a new state-of-the-art performance.

1 Introduction

Black-box optimisation arises in scientific and engineering domains where evaluating each candidate solution is costly, often requiring extensive physical experiments or high-fidelity simulations [45]. For instance, designing energy-efficient hardware accelerators [4, 7, 27] involves numerous cycle-accurate simulations to assess configuration performance. In materials science, finding nanoporous structures with high adsorption capacity for carbon capture or hydrogen storage demands labor-intensive lab

*These authors contributed equally.

[†]Corresponding authors: Manh Cuong Dao, The Hung Tran, Trong Nghia Hoang.

experiments [15, 18]. Similar challenges arise in protein design [19], molecular generation [14], and drug discovery [38], where evaluations are likewise expensive.

Prior Literature. Existing approaches to black-box optimization include both online and offline methods with the latter being an emerging alternative of the former. In particular, online methods such as Bayesian optimization [39, 40, 46, 47, 48, 49] have long been explored for black-box design tasks with provable performance guarantee in the asymptotic limit of data. However, their reliance on iterative experimentation makes them less practical in high-cost settings with limited to no experimentation budget. In contrast, black-box methods leverage past data to learn a surrogate model which can be used to find better designs without incurring new experimentation [26, 6, 16, 10, 24, 30, 43, 44]. In this paper, we focus on the offline setting, where the goal is to discover high-performing designs using only past experimentation data.

Challenge. Among offline methods, the main challenge is that surrogate models can become increasingly erroneous when the search moves away from the offline dataset, especially when offline data are biased or sparse, causing these models to overfit. To mitigate this issue, most existing approaches have focused on advancing techniques in (1) **forward modeling** that penalize high-value surrogate predictions at out-of-distribution (OOD) inputs [44, 11, 54], (2) **inverse modeling** that find most promising and reliable regions that contain high-performing inputs [30, 33, 29, 8] to sidestep the OOD issue of forward modeling, and (3) **search policies** that learn a direct plan to navigate from low-value inputs to high-value inputs [8, 28].

Limitations. Despite their promising results, forward and inverse approaches depend on learning a mapping (or inverse mapping) between input designs and their corresponding performance outputs using offline data. As a result, their effectiveness is inherently limited by the availability of data. Likewise, learning direct search policies also suffers from the same data bottleneck since these methods still need to sample heuristic trajectories from the offline dataset to use as learning feedback.

Furthermore, information regarding regions with high-performing inputs is often not observable from the offline data, especially in low-data scenarios which might further restrict the effectiveness of the learned models/policies. To mitigate such data bottleneck, we propose to approach offline optimization from a *new perspective of distributional translation*, as highlighted below.

Distributional Translation. In essence, we view the offline data as an implicit distribution over low-value designs, and recast offline optimization as the task of learning a probabilistic transformation, or bridge, that transports this distribution toward a regime of higher-value inputs. By moving along the learned probabilistic bridge, we can reach regions of the input space associated with better designs. However, learning such a transformation is fundamentally limited by the scarcity of high-value examples. Our key insight to overcome this bottleneck is:

Although the feedback needed to learn such low-to-high probabilistic transformation is absent in the offline dataset, it can be derived from a distribution of synthetic functions that are similar to the (unknown) target function (up to a scale factor).

These synthetic functions can be provably constructed across various output scales, alleviating the data bottleneck and broadening the solution scope of offline optimization.

Technical Contributions. Our solution perspective is substantiated via the following:

1. A general-purpose probabilistic bridge model that learns a direct mapping between two implicit data distributions. This perspective rethinks offline optimization through the lens of probabilistic transport. The resulting bridge can incorporate external guiding information from synthetic functions similar to the oracle to mitigate the data bottleneck. Once trained, it enables simulation of paths that move from low-value to high-value regimes (Section 3.1).
2. A pre-training and adaptation framework that (1) learns multiple Gaussian process priors [50] over synthetic functions resembling the target function, and (2) samples representative low- and high-value inputs from their corresponding closed-form mean functions. This generates high-quality training data that better delineate the low- and high-value regimes for learning the probabilistic bridge. The intuition is that if the bridge can consistently map between these regimes across a wide range of functions similar to the oracle, it will be able to do the same for the oracle (Section 3.3).

3. An extensive empirical evaluation on a variety of benchmark datasets [43] and numerous existing baselines, establishing a new state-of-the-art performance, which significantly and consistently improves over previous work. Our empirical evaluation also features rich ablation studies examining in detail the practical impact of different components of our framework on its performance (Section 4).

2 Problem Definition and Preliminaries

This section provides a concise formulation of offline black-box optimization (Section 2.1) and important background on Gaussian processes (Section 2.2) which was used later for sampling additional data from synthetic functions similar to the oracle behind the offline data.

2.1 Offline Black-Box Optimization

Offline black-box optimization is formulated as the maximization of a black-box function $f(\mathbf{x})$ using only an offline dataset of observations $D_o = \{(\mathbf{x}_i, y_i)\}_{i=1}^n$ which \mathbf{x}_i denote a past experiment design and $y_i = f(\mathbf{x}_i)$ is its corresponding evaluation. A direct approach to this problem is to learn a surrogate $g(\mathbf{x}; \boldsymbol{\omega}_*)$ of $f(\mathbf{x})$ via fitting its parameter $\boldsymbol{\omega}_*$ to the offline dataset,

$$\boldsymbol{\omega}_* \triangleq \arg \min_{\boldsymbol{\omega}} L(\boldsymbol{\omega}) \triangleq \arg \min_{\boldsymbol{\omega}} \sum_{i=1}^n \ell(g(\mathbf{x}_i; \boldsymbol{\omega}), y_i), \quad (1)$$

where $\boldsymbol{\omega}$ denotes a parameter candidate of the surrogate and $\ell(g(\mathbf{x}; \boldsymbol{\omega}), y)$ denotes the prediction loss of $g(\cdot; \boldsymbol{\omega})$ on \mathbf{x} if its oracle output is y . The (oracle) maxima of $f(\mathbf{x})$ is then approximated via,

$$\mathbf{x}_* \triangleq \arg \max_{\mathbf{x}} g(\mathbf{x}; \boldsymbol{\omega}_*). \quad (2)$$

The main issue with this approach is that $g(\mathbf{x}; \boldsymbol{\omega}_*)$ often predicts erratically at out-of-distribution (OOD) inputs. To mitigate this, numerous surrogate or search regularizers have been proposed to either penalize the high-value surrogate prediction at OOD inputs [11, 44, 54] or find an inverse mapping from the desired output to potential inputs [29, 33], as detailed in Section 5. Nonetheless all these approaches are restricted by the limited amount of offline data. Alleviating this bottleneck to reach new SOTA performance is main aim of our proposed approach.

2.2 Gaussian Processes

A Gaussian process (GP) [36] defines a probabilistic prior over a random function $h(\mathbf{x})$. It is parameterized by a mean function $m(\mathbf{x}) = 0^3$ and a kernel function $k(\mathbf{x}, \mathbf{x}')$. These functions induce a marginal Gaussian prior over the evaluations $\mathbf{h} = [h(\mathbf{x}_1) \dots h(\mathbf{x}_n)]^\top$ of any finite subset of inputs $\{\mathbf{x}_1, \dots, \mathbf{x}_n\}$. Let \mathbf{x}_τ be an unseen input whose corresponding output $h_\tau = h(\mathbf{x}_\tau)$ we wish to predict. The Gaussian prior over $[h(\mathbf{x}_1) \dots h(\mathbf{x}_n) \ h(\mathbf{x}_\tau)]^\top$ implies:

$$h(\mathbf{x}_\tau) \mid \mathbf{h} \sim \mathbb{N}(\mathbf{k}_\tau^\top \mathbf{K}^{-1} \mathbf{h}, k(\mathbf{x}_\tau, \mathbf{x}_\tau) - \mathbf{k}_\tau^\top \mathbf{K}^{-1} \mathbf{k}_\tau), \quad (3)$$

where $\mathbf{k}_\tau = [k(\mathbf{x}_\tau, \mathbf{x}_1) \dots k(\mathbf{x}_\tau, \mathbf{x}_n)]^\top$ and \mathbf{K} denotes the Gram matrix induced on $\{\mathbf{x}_1, \dots, \mathbf{x}_n\}$ for which $\mathbf{K}_{ij} = k(\mathbf{x}_i, \mathbf{x}_j)$. Assuming a Gaussian likelihood $y \sim \mathbb{N}(h(\mathbf{x}), \sigma^2)$, it follows that

$$h(\mathbf{x}_\tau) \mid \mathbf{y} \sim \mathbb{N}(\mathbf{k}_\tau^\top (\mathbf{K} + \sigma^2 \mathbf{I})^{-1} \mathbf{y}, k(\mathbf{x}_\tau, \mathbf{x}_\tau) - \mathbf{k}_\tau^\top (\mathbf{K} + \sigma^2 \mathbf{I})^{-1} \mathbf{k}_\tau), \quad (4)$$

which explicitly forms the predictive distribution of a Gaussian process. The choice of the kernel function $k(\mathbf{x}, \mathbf{x}')$ dictates certain properties of the sample functions. In this context, we adopt the commonly used RBF kernel, $k(\mathbf{x}, \mathbf{x}') = \sigma^2 \exp(-0.5 \cdot \|\mathbf{x} - \mathbf{x}'\|^2 / \ell^2)$ with the parameter σ^2 represents the signal variance, controlling the function's amplitude, while ℓ denotes the unit length-scale which regulates the function's smoothness.

3 Rethinking Offline Optimization as Distributional Translation

This section introduces a new perspective on offline optimization by framing it as a translation task. We intuitively view the offline data as a source language composed of low-value designs

³We assume a zero mean function since the output can always be re-centered around 0.

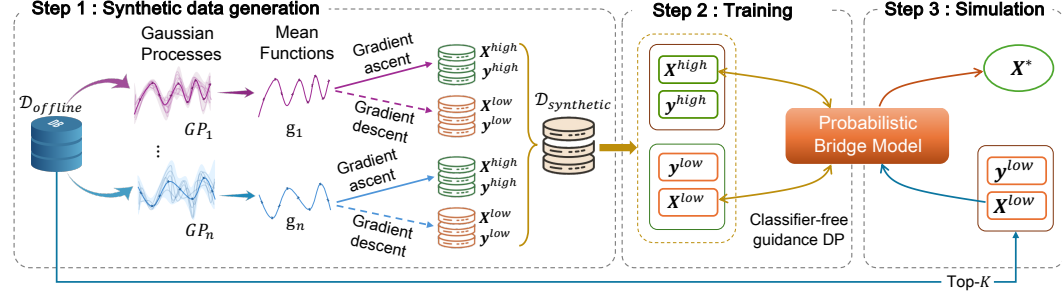


Figure 1: Overview of the **ROOT** workflow: (1) Multiple Gaussian process posteriors are fitted to the offline data, and low- and high-value inputs from the posterior mean functions are sampled to construct a synthetic dataset. (2) This dataset is used to construct our probabilistic bridge model, which learns to map between two different implicit data distributions. (3) The backward process of the learned bridge model is applied to the top-performing inputs from the offline data to generate high-quality candidates for the unknown target function.

and aim to translate it into a target language of high-value inputs. To enable this translation, we introduce the concept of a probabilistic bridge which identifies local translation examples by explicitly conditioning on both the source and target contexts. This conditioning enables the construction of feasible transformation paths that connect selected low- and high-value designs within their local neighborhoods, grounding the translation process in meaningful design correspondences (Section 3.1).

These local bridges serve as examples of how to move between regimes when both endpoints are known. The learning algorithm then weaves together these examples to form a global translator capable of generalizing beyond the observed pairs and enabling translation in new contexts where expectedly only the source is known. This approach generalizes diffusion models [22], which translate between data and noise, and allows external guiding information to be incorporated, enriching the context and addressing the data bottleneck in offline optimization (Section 3.3).

3.1 Probabilistic Bridge for Distributional Translation

This section formalizes the concept of a probabilistic bridge, which generalizes the widely used Denoising Diffusion Probabilistic Model (DDPM) [22]. While DDPM defines a forward diffusion process that maps data to Gaussian noise and learns to reverse it, the probabilistic bridge constructs a space of localized transformation flows conditioned on both the source and the target, representing low-value and high-value designs drawn from implicit data distributions. Learning and applying a probabilistic bridge model for distributional translation involves two phases: a construction phase (Section 3.1) and a learning phase (Section 3.3).

In the construction phase, the transition kernel of each conditioned bridge is derived, capturing a source-to-target translation plan within its local context. These localized examples serve as concrete demonstrations of how to move between regimes. In the learning phase, they are used to train a global, target-agnostic transformation flow that generalizes beyond the observed pairs and enables translation from arbitrary source inputs to valid target outputs. These two phases are described in detail below. A concrete example of a probabilistic bridge is also given in Section 3.2.

3.1.1 Probabilistic Bridge Construction

Given two endpoints \mathbf{x}_0 and \mathbf{x}_T , we define a *probabilistic bridge* between them as a discrete observation of a vector-value, time-indexed random function $\mathbf{x}_1, \mathbf{x}_2, \dots, \mathbf{x}_{T-1}$ which is distributed by Gaussian process [36] with mean function $\psi_t(\mathbf{x}_0, \mathbf{x}_T)$ and covariance kernel $\kappa_{t,k} \mathbf{I}$ ⁴.

This implies a marginal Gaussian on the probabilistic bridge $\mathbf{x} = \text{vec}[\mathbf{x}_1, \mathbf{x}_2, \dots, \mathbf{x}_{T-1}]$ with mean $\psi = \text{vec}[\psi_1(\mathbf{x}_0, \mathbf{x}_T); \dots; \psi_{T-1}(\mathbf{x}_0, \mathbf{x}_T)]$ which reveals a mass-moving flow between \mathbf{x}_T and \mathbf{x}_0 ,

$$q(\mathbf{x} | \mathbf{x}_0, \mathbf{x}_T) \triangleq \mathbb{N}(\mathbf{x}; \psi, \kappa \otimes \mathbf{I}) \Rightarrow q(\mathbf{x}_t | \mathbf{x}_0, \mathbf{x}_T) = \mathbb{N}(\mathbf{x}_t; \psi_t(\mathbf{x}_0, \mathbf{x}_T), \kappa_{t,t} \mathbf{I}), \quad (5)$$

⁴We use $\kappa_{t,k} \mathbf{I}$ to denote the cross-covariance matrix between \mathbf{x}_t and \mathbf{x}_k under the joint distribution.

where \otimes denotes the Kronecker product, κ is a matrix containing the entries $\kappa_{t,k}$ and the mean function $\psi_t(\mathbf{x}_0, \mathbf{x}_T)$ must meet boundary conditions $\psi_0(\mathbf{x}_0, \mathbf{x}_T) = \mathbf{x}_0$ and $\psi_T(\mathbf{x}_0, \mathbf{x}_T) = \mathbf{x}_T$. This further reveals a closed-form expression for backward transition conditioned on both endpoints,

$$q(\mathbf{x}_{t-1} | \mathbf{x}_t, \mathbf{x}_0, \mathbf{x}_T) = \mathbb{N}(\mathbf{x}_{t-1}; \boldsymbol{\mu}(\mathbf{x}_t, \mathbf{x}_0, \mathbf{x}_T), \tilde{\kappa}_{t-1} \mathbf{I}), \quad (6)$$

with the transition mean $\boldsymbol{\mu}(\mathbf{x}_t, \mathbf{x}_0, \mathbf{x}_T) = \psi_{t-1}(\mathbf{x}_0, \mathbf{x}_T) + \kappa_{t-1,t} \kappa_{t,t}^{-1} (\mathbf{x}_t - \psi_t(\mathbf{x}_0, \mathbf{x}_T))$ and covariance $\tilde{\kappa}_{t-1} = \kappa_{t-1,t-1} - \kappa_{t-1,t} \kappa_{t,t}^{-1} \kappa_{t,t-1}$. This reveals a (step-wise) conditional backward transition that induces a valid transformation flow mapping \mathbf{x}_T back to \mathbf{x}_0 . This means for each sampled pair $(\mathbf{x}_T, \mathbf{x}_0)$, the corresponding target-conditioned backward transition $q(\mathbf{x}_{t-1} | \mathbf{x}_t, \mathbf{x}_0, \mathbf{x}_T)$ provides an example of a localized transformation flow between them, which can be used to train the desired target-agnostic map $p_\theta(\mathbf{x}_{t-1} | \mathbf{x}_t, \mathbf{x}_T)$ as detailed next.

3.1.2 Learning Probabilistic Bridge Model

To learn the target-agnostic transformation that maps from a source to a plausible target without knowing it beforehand, we parameterize it as

$$p_\theta(\mathbf{x}_{t-1} | \mathbf{x}_t, \mathbf{x}_T) = \mathbb{N}(\mathbf{x}_{t-1}; \boldsymbol{\mu}_\theta(\mathbf{x}_t, \mathbf{x}_T, t), \tilde{\kappa}_{t-1} \mathbf{I}), \quad (7)$$

which uses the same (known) variance parameter as the localized flow/bridge example above and a (learnable) spatio-temporal network $\epsilon_\theta(\mathbf{x}_t, t)$ to parameterize the target-agnostic mean transition. This is the centerpiece of the probabilistic bridge model in Eq. 7 which can now be learned via optimizing its parameter θ to match the example flows generated using Eq. 6,

$$\theta_{\text{PB}} = \arg \min_{\theta} \mathbb{E}_{(\mathbf{x}_0, \mathbf{x}_T, t)} \left[\text{D}_{\text{KL}} \left(q(\mathbf{x}_{t-1} | \mathbf{x}_t, \mathbf{x}_0, \mathbf{x}_T) \| p_\theta(\mathbf{x}_{t-1} | \mathbf{x}_t, \mathbf{x}_T) \right) \right]. \quad (8)$$

The KL divergence in Eq. 8 above is between two Gaussians and can be computed in closed form which allows for a direct optimization of θ . Given the optimized θ_{PB} and a source \mathbf{x}_T (low-value design), we can now simulate the generic transformation flow in Eq. 7 to obtain a plausible target \mathbf{x}_0 (high-value design) which is not known apriori,

$$\mathbf{x}_{t-1} = \boldsymbol{\mu}_{\theta_{\text{PB}}}(\mathbf{x}_t, \mathbf{x}_T, t) + \sqrt{\tilde{\kappa}} \epsilon, \quad (9)$$

where we sample $\epsilon \sim \mathbb{N}(0, \mathbf{I})$ when $t > 1$ and set $\epsilon = 0$ otherwise. This gives us the desired transformation that translates a candidate in the low-value regime to another in the high-value regime. Furthermore, to improve training efficiency, we can also adopt the practical approach in guided diffusion which further conditions $\boldsymbol{\mu}_\theta(\mathbf{x}_t, \mathbf{x}_T, t) = \boldsymbol{\mu}_\theta(\mathbf{x}_t, \mathbf{x}_T, y_0, y_T, t)$ on the source and target outputs (i.e., y_T and y_0) [23].

3.2 Example and Practical Setup

This section provides an working example to substantiate the above probabilistic bridge framework. Choosing $\psi_t(\mathbf{x}_0, \mathbf{x}_T) = \mathbf{x}_0(1-t/T) + \mathbf{x}_T(t/T)$ and $\kappa_{t,k} = (\min(t, k)/T)(1-\max(t, k)/T)$ results in a Brownian bridge construction,

$$q(\mathbf{x}_t | \mathbf{x}_0, \mathbf{x}_T) = \mathbb{N} \left(\mathbf{x}_t; \mathbf{x}_0 \left(1 - \frac{t}{T} \right) + \mathbf{x}_T \frac{t}{T}, \frac{t}{T} \left(1 - \frac{t}{T} \right) \mathbf{I} \right). \quad (10)$$

This specifies a transport plan that moves the unit point mass located as \mathbf{x}_T to \mathbf{x}_0 . To see this, note that when $t = 0$, Eq. 10 reduces to $\mathbb{N}(\mathbf{x}_0, 0)$ and when $t = T$, it reduces to $\mathbb{N}(\mathbf{x}_T, 0)$. This setup emphasizes a point-to-point transformation which is particularly suitable for offline optimization.

As we substantiate Eq. 10 with the appropriate (low-value, high-value) pairs $(\mathbf{x}_T, \mathbf{x}_0)$ and derive examples of localized flow mapping from the low- and high-value regimes following the blueprint in Section 3.1.1, we can learn a target-agnostic transformation consistent with using Eq. 8. This setup has been used in our experiments to achieve significant performance improvement over prior work, effectively establishing new SOTA. Further details regarding the specific derivation of the Brownian bridge and its practical traning procedure is detailed in Appendix B.2.

Remark. The above framework offers a broad and flexible perspective on offline optimization that has not been fully explored in the existing literature. From this viewpoint, there are many promising

directions for future investigation. Each valid specification of the mean and kernel functions in the probabilistic bridge model in Eq. 5 defines a distinct way of transporting probability mass from low-value to high-value regions. While offline optimization ultimately requires only one such transport plan, different choices may lead to significantly different learning behaviors and complexities. Understanding how the choice of bridge design influences learning performance remains an important and open question for future work.

▷ Learning θ_{PB} however requires access to paired samples of low-value and high-value designs, which is nontrivial in the offline optimization setting where the dataset typically reflects only the low-value regime. This raises a fundamental question: *where can we obtain representative samples from the high-value regime to support bridge construction?* Addressing this challenge is critical for making the probabilistic bridge framework operational, and is the focus of Section 3.3.

3.3 Synthetic Data Generation and Practical Black-Box Optimization Algorithm: ROOT

This section revisits the challenge introduced in Section 1: Learning a probabilistic bridge requires examples of localized flows from low- to high-value regimes. Yet, such examples are not available in standard offline datasets, which by design lack high-performing solutions. To address this, we propose a key hypothesis: if a probabilistic bridge can consistently translate low-value inputs to high-value outputs across a sufficiently large set of functions similar to the oracle, it is likely to generalize well to the oracle.

Motivation. This motivates an alternative data generation strategy. Rather than depending solely on the offline dataset, we construct a collection of synthetic functions with closed-form structure, allowing us to sample large quantities of low- and high-value inputs. These synthetic examples enable us to train a meta probabilistic bridge with strong zero-shot adaptation. This strategy reflects the common pre-training paradigm in foundation model development, where knowledge accumulated from broad synthetic tasks can be readily transferred to any target task of interest. This motivation leads to our overall workflow, which is illustrated in Figure 1.

Function Sampling. Collecting data from such similar functions is fortunately possible using the Gaussian process [36] which specifies a prior over functions around a given mean function. Assuming that the mean function is set to be the oracle, most sampled functions from the corresponding GP will be similar to it. Since we do not know the oracle function, another approach is to begin with a generic GP prior with kernel parameters $\phi = (\sigma, \ell)$ and compute the corresponding GP posterior using the offline data D_o . The resulting GP posterior mean is

$$\bar{g}_{\phi_s}(\mathbf{x}) = \mathbf{k}(\phi_s)^\top (\mathbf{K}(\phi_s) + \sigma^2 \mathbf{I})^{-1} \mathbf{y}, \quad (11)$$

which has a closed form and is similar the oracle function around the offline data D_o . To obtain a wider range of functions similar to the oracle, we compute multiple GP posteriors according to a diverse range of GP priors with different signal and length-scale parameters. These can be obtained from learning a hierarchical GP prior with top-level prior over kernel parameters defining the corresponding GP posteriors at the lower level. We can then sample kernel parameters $\{\phi_s\}_{s=1}^{n_g}$ and extract the corresponding posterior means – see Eq. 11.

Low- and High-Value Simulation. Given these functions, we can construct \mathbf{X}_s^- and \mathbf{X}_s^+ as the set of low- and high-value inputs of $\bar{g}_{\phi_s}(\mathbf{x})$ via running M -step gradient descent and ascent from a subset of n_p offline input points:

$$\mathbf{X}_s^- \triangleq \left\{ \mathbf{x}_M^- \triangleq \mathbf{x}_0^- - \eta \sum_{m=0}^{M-1} \nabla_{\mathbf{x}} \bar{g}_{\phi_s}(\mathbf{x}_m^-) \mid \mathbf{x}_0^- \in \mathcal{D}_0 \right\}, \quad (12)$$

$$\mathbf{X}_s^+ \triangleq \left\{ \mathbf{x}_M^+ \triangleq \mathbf{x}_0^+ + \eta \sum_{m=0}^{M-1} \nabla_{\mathbf{x}} \bar{g}_{\phi_s}(\mathbf{x}_m^+) \mid \mathbf{x}_0^+ \in \mathcal{D}_0 \right\}, \quad (13)$$

where $\mathbf{x}_{m+1}^+ \triangleq \mathbf{x}_m^+ + \eta \nabla_{\mathbf{x}} \bar{g}_{\phi_s}(\mathbf{x}_m^+)$ and $\mathbf{x}_{m+1}^- \triangleq \mathbf{x}_m^- - \eta \nabla_{\mathbf{x}} \bar{g}_{\phi_s}(\mathbf{x}_m^-)$. Here, $\mathbf{x}_0^+ = \mathbf{x}_0^- \in D_o$. The corresponding outputs for the above inputs can also be computed using the closed-form of the posterior means. A synthetic dataset D_s collecting low- and high-values from those closed-form posterior mean functions can then be created:

$$D_s = \left\{ (\mathbf{X}_s^-, \mathbf{y}_s^-), (\mathbf{X}_s^+, \mathbf{y}_s^+) \right\}_{s=1}^{n_g} \quad \text{where} \quad \mathbf{y}_s^- = \bar{g}_{\phi_s}(\mathbf{X}_s^-) \quad \text{and} \quad \mathbf{y}_s^+ = \bar{g}_{\phi_s}(\mathbf{X}_s^+), \quad (14)$$

where n_g is the number of sampled functions.

Learning Probabilistic Bridge. Following the blueprint in Section 3.1.1, we can sample $(\mathbf{x}_T, y_T, \mathbf{x}_0, y_0) \sim D_s$ as training data to train our probabilistic bridge mapping between low- and high-value regions across the aforementioned posterior mean functions, which follows Eq. 8. Furthermore, we also adopt the guided diffusion [23] technique to incorporate the output information y_T and y_0 as part of the input to the prediction network $\mu_\theta(\mathbf{x}_t, \mathbf{x}_T, y_0, y_T, t)$ as stated after Eq. 9.

Simulation. Once this probabilistic bridge model has been trained, we can utilize its corresponding (step-wise) source-to-target transition in Eq. 9 to map each offline input (presumably in the low-value regime) to a better solution candidate (in a high-value regime). For example, we can run this simulation for the top 128 offline inputs with highest values. The effectiveness of this approach is thoroughly evaluated in Section 4, where we demonstrate its ability to generate high-quality candidates across various benchmarks. A full description of our algorithm and implementation is presented in Appendix B. Our algorithm’s computational complexity is discussed in Appendix C.4.

4 Experiments

This section evaluates our proposed method, **ROOT**, through extensive empirical comparisons against various recent baselines on a standard offline optimization benchmark [43]. The experiment setup is summarized in Section 4.1, with detailed results in Section 4.2 and ablation studies in Section 4.3.

4.1 Experiments Settings

Benchmark Tasks. Our investigation covers four real-world tasks selected from the Design-Bench [43]⁵ and three RNA-Binding tasks from ViennaRNA [32]. In Design-Bench, the chosen tasks cover both discrete and continuous domains. The discrete tasks, **TF-Bind-8** and **TF-Bind-10** [3], aim to discover DNA sequences with high binding affinity to a specific transcription factor (SIX6 REF R1). On the continuous side, **Ant Morphology** [5] and **D’Kitty Morphology** [2] focus on optimizing the physical structure of a simulated robot ant from OpenAI Gym [5] and the D’Kitty robot from ROBEL [2]. For ViennaRNA, we include three RNA-Binding tasks as RNA-A, RNA-B, and RNA-C [32, 25]. For further details on these tasks, please read Appendix A.

Baselines. We selected 21 widely recognized offline optimizers for comparison, including **BO-qEI** [43], **CMA-ES** [21], **REINFORCE** [51], **COMs** [44], **CbAS** [6], **MINs** [30], **RoMA** [53], **DDOM** [29], **ICT** [54], **Tri-mentoring** [11], **GTG** [56], **BDI** [10], **RGD** [9], **LTR** [41], **BONET** [28], **MATCH-OPT** [24], **PGS** [8], **GABO** [52], **DEMO** [55], **GA on GP** (Section 4.3) and standard **GA**.

Evaluation Protocol. Following the approach in [43], each method generates 128 optimized design candidates, which are then evaluated by the oracle function. The performances are ranked, and results are recorded at the 50th, 80th, and 100th percentiles. To ensure consistency, all results are averaged over 8 independent runs with reported standard deviation.

Hyper-parameter Configuration. For each baseline, we adopt the optimized settings from the original papers. For GP kernel hyper-parameters in our data generation, we sample lengthscales ℓ_s and variances σ_s^2 uniformly from $[\ell_0 - \delta, \ell_0 + \delta]$ and $[\sigma_0^2 - \delta, \sigma_0^2 + \delta]$, with $\ell_0 = \sigma_0^2 = 1.0$ for continuous tasks and 6.25 for discrete tasks, and $\delta = 0.25$. We use $M = 100$ gradient steps with step sizes 0.001 (continuous) and 0.05 (discrete). Additional data generation details are in Appendix B.1 and Table 6. For training the Probabilistic Bridge model, we use a Brownian Bridge diffusion process with the Adam optimizer over $E = 100$ epochs and $n_g = 800$ synthetic functions, running on a single NVIDIA A100-SXM4-80GB GPU. More training details are provided in Appendix B.2.

4.2 Experimental Results

This section compares our method to 21 baselines, evaluating the 50th, 80th, and 100th percentiles. Due to limited space, we report only the 100th percentile results in the main text; details on the 50th and 80th percentiles and score distributions for our method versus others are in Appendix C.2.

⁵We exclude tasks marked by previous works as having high oracle function noise and inaccuracy (**ChEMBL**, **Hopper**, and **Superconductor**) and tasks require substantial computational resources to evaluate (**NAS**)

Table 1: Experiment results on Design-Bench Tasks. We report the maximum score (100th percentile) among $Q = 128$ candidates. **Blue** denotes the best entry in the column, while **Brown** indicates the second best. **Mean Rank** is the average rank across all benchmark tasks.

Method	Benchmarks				Mean Rank
	Ant	D'Kitty	TFBind8	TFBind10	
D_o (best)	0.565	0.884	0.439	0.467	-
BO-qEI	0.812 ± 0.000	0.896 ± 0.000	0.825 ± 0.091	0.627 ± 0.033	16.75 / 22
CMA-ES	1.561 ± 0.896	0.724 ± 0.001	0.939 ± 0.039	0.664 ± 0.034	8.00 / 22
REINFORCE	0.263 ± 0.026	0.573 ± 0.204	0.961 ± 0.034	0.618 ± 0.011	17.00 / 22
GA	0.293 ± 0.029	0.860 ± 0.021	0.985 ± 0.011	0.638 ± 0.032	12.75 / 22
COMs	0.882 ± 0.044	0.932 ± 0.006	0.940 ± 0.027	0.621 ± 0.033	13.25 / 22
CbAS	0.846 ± 0.033	0.895 ± 0.016	0.903 ± 0.028	0.649 ± 0.055	12.50 / 22
MINs	0.894 ± 0.022	0.939 ± 0.004	0.908 ± 0.063	0.630 ± 0.019	12.50 / 22
GA on GP	0.948 ± 0.013	0.946 ± 0.001	0.770 ± 0.087	0.654 ± 0.038	9.25 / 22
RoMA	0.593 ± 0.066	0.829 ± 0.020	0.665 ± 0.000	0.553 ± 0.000	20.00 / 22
ICT	0.911 ± 0.030	0.945 ± 0.011	0.888 ± 0.047	0.624 ± 0.033	13.50 / 22
Tri-mentoring	0.944 ± 0.033	0.950 ± 0.015	0.899 ± 0.045	0.647 ± 0.039	9.00 / 22
MATCH-OPT	0.931 ± 0.011	0.957 ± 0.014	0.977 ± 0.004	0.543 ± 0.002	9.50 / 22
PGS	0.949 ± 0.017	0.966 ± 0.013	0.981 ± 0.015	0.532 ± 0.000	7.75 / 22
LTR	0.907 ± 0.032	0.960 ± 0.014	0.973 ± 0.000	0.652 ± 0.039	6.25 ± 22
DDOM	0.930 ± 0.029	0.925 ± 0.008	0.885 ± 0.061	0.634 ± 0.015	13.75 / 22
GTG	0.865 ± 0.040	0.935 ± 0.010	0.901 ± 0.039	0.639 ± 0.016	12.50 / 22
BDI	0.964 ± 0.000	0.941 ± 0.000	0.973 ± 0.000	0.636 ± 0.020	7.50 / 22
RGD	0.922 ± 0.020	0.883 ± 0.014	0.889 ± 0.068	0.644 ± 0.048	13.00 / 22
BONET	0.948 ± 0.025	0.957 ± 0.008	0.894 ± 0.086	0.606 ± 0.024	10.75 / 22
GABO	0.224 ± 0.051	0.719 ± 0.001	0.939 ± 0.038	0.639 ± 0.033	15.25 / 22
DEMO	0.948 ± 0.013	0.956 ± 0.011	0.812 ± 0.054	0.648 ± 0.042	9.25 / 22
ROOT (ours)	0.965 ± 0.014	0.972 ± 0.005	0.986 ± 0.007	0.685 ± 0.053	1.25 ± 22

Table 2: Experiments on Biological RNA Design Tasks. We report the maximum score among $Q = 128$ candidates.

Method	Benchmarks			Mean Rank
	RNA-A	RNA-B	RNA-C	
CbAS	0.270 ± 0.098	0.249 ± 0.088	0.261 ± 0.093	6.00 / 8
BO-qEI	0.537 ± 0.106	0.517 ± 0.108	0.481 ± 0.100	3.67 / 8
GA	0.518 ± 0.120	0.499 ± 0.100	0.496 ± 0.091	4.33 / 8
COMs	0.187 ± 0.123	0.144 ± 0.121	0.209 ± 0.100	7.67 / 8
REINFORCE	0.166 ± 0.096	0.149 ± 0.081	0.225 ± 0.075	7.33 / 8
BDI	0.604 ± 0.000	0.505 ± 0.000	0.411 ± 0.000	4.00 / 8
Boot-Gen	0.913 ± 0.064	0.881 ± 0.024	0.786 ± 0.039	2.00 ± 8
ROOT (ours)	0.956 ± 0.023	0.955 ± 0.013	0.922 ± 0.013	1.00 ± 8

Table 3: Effect of initial-point selection on **ROOT**'s performance.

Type	Ant	TFBind8
Random	0.953 ± 0.014	0.976 ± 0.007
Lowest	0.545 ± 0.214	0.969 ± 0.009
Highest	0.965 ± 0.014	0.986 ± 0.007

Table 4: **ROOT** vs ExPT in few-shot settings.

Method	Ant	TFBind8
ExPT	0.940 ± 0.027	0.874 ± 0.071
ROOT	0.942 ± 0.035	0.895 ± 0.086

Results on Continuous Tasks: Table 1 (first two columns) shows our continuous-task results. On D'Kitty we set a new SOTA at **0.972** with a small standard deviation **0.005**. On Ant, although CMA-ES surpasses us at the 100th percentile, its standard deviation (**0.896**) is nearly **64**× ours (**0.014**) and it collapses near zero at the 80th/50th percentiles (see Appendix C.2).

Results on Discrete Tasks: Table 1 (last two columns) present our discrete-task results. Our **ROOT** achieves both the top rank for the TFBInd10 task with a mean score **0.685** and TFBInd8 task with **0.986**. Our standard deviation **0.007** for the TFBInd8 task is even smaller than that of all other baselines, except for RoMa, which performs poorly.

Results on RNA-Binding Tasks: Table 2 demonstrates **ROOT**'s superior performance, ranking first on all three RNA benchmarks. We outperform Boot-Gen[25] by margins of **0.043** (RNA-A), **0.074** (RNA-B), and **0.136** (RNA-C), while our standard deviations are roughly half those of Boot-Gen, achieving better performance and lower variance (hence, more stable).

Table 5: Performance on **TF-Bind-8** and **Ant** of different methods trained by only the $p\%$ poorest-performing designs from the offline dataset.

Method	TF-Bind-8			Ant		
	50%	20%	10%	50%	20%	10%
GA	0.580 ± 0.199	0.480 ± 0.218	0.559 ± 0.170	0.394 ± 0.023	0.663 ± 0.065	0.619 ± 0.120
COMs	0.935 ± 0.052	0.872 ± 0.085	0.771 ± 0.128	0.898 ± 0.035	0.880 ± 0.027	0.845 ± 0.041
REINFORCE	0.915 ± 0.039	0.917 ± 0.040	0.913 ± 0.038	0.317 ± 0.016	0.261 ± 0.052	0.281 ± 0.034
LTR	0.959 ± 0.022	0.927 ± 0.033	0.909 ± 0.034	0.909 ± 0.042	0.871 ± 0.059	0.813 ± 0.026
ROOT	0.964 ± 0.015	0.946 ± 0.045	0.915 ± 0.019	0.909 ± 0.012	0.930 ± 0.023	0.861 ± 0.051

Table 6: Impact of gradient steps M on **ROOT**.

Steps (M)	Ant	D'Kitty	TF-Bind-8	TF-Bind-10
25	0.968 ± 0.009	0.972 ± 0.003	0.952 ± 0.024	0.640 ± 0.039
50	0.968 ± 0.015	0.969 ± 0.003	0.945 ± 0.025	0.639 ± 0.024
75	0.950 ± 0.011	0.969 ± 0.005	0.972 ± 0.013	0.652 ± 0.033
100	0.965 ± 0.014	0.972 ± 0.005	0.986 ± 0.007	0.685 ± 0.053

Table 7: Impact of number of initial data points on **ROOT**.

Initial Points (n_p)	Ant	TF-Bind-8
128	0.915 ± 0.020	0.948 ± 0.024
256	0.950 ± 0.010	0.968 ± 0.018
512	0.964 ± 0.010	0.974 ± 0.006
1024	0.965 ± 0.014	0.986 ± 0.007

Overall, **ROOT** achieved a mean rank of **1.25** across both discrete and continuous domains, setting a new SOTA on 3 out of 4 Design-Bench tasks, as well as on all three RNA-binding tasks. This demonstrates the robust and consistent effectiveness of **ROOT** across diverse settings.

4.3 Ablation Experiments

Selection Strategies for Initial Points. We explore 3 initial point strategies for $\mathbf{x}_0^+, \mathbf{x}_0^-$ in (Eq. 12 and Eq. 13): random sampling, and selecting points with the lowest or highest objective values from D_o . As shown in Table 3, the third strategy achieves the best results.

Few-Shot Experimental Designs Setting. In offline optimization, the few-shot experimental designs (ED) setting, introduced in ExPT [33], presents a more challenging task where only a small set of labeled data points, $D_{\text{label}} = \{(\mathbf{x}_i, y_i)\}_{i=1}^{n_l}$ is available alongside a larger set of unlabeled data, $D_{\text{unlabeled}} = \{\mathbf{x}_i\}_{i=1}^{n_u}$. To evaluate our model in this scenario, we follow ExPT’s protocol, using a random 1% of the offline data as labeled points and the remaining 99% as unlabeled. For synthetic function generation, we first fit a prior Gaussian Process (GP) to D_{label} , then use the posterior to generate pseudo-labels for $D_{\text{unlabeled}}$. We combine the labeled and pseudo-labeled data and fit another GP to this dataset. The mean function of this refitted GP is used as the synthetic function, following the same procedure as in the main method. As shown in Table 4, **ROOT** outperforms the ExPT model in this setting by substantial margins.

Poor Offline data Coverage Setting. Beyond the Few-Shot Experimental Design scenario with limited coverage, we further evaluated **ROOT**’s robustness under varying dataset support quality. Specifically, we trained **ROOT** and the baselines using only the $p\%$ lowest-performing designs from the offline dataset. As shown in Table 5, **ROOT** achieves the best performance across all settings on both **TF-Bind-8** and **Ant**. These results demonstrate that **ROOT** adapts effectively in challenging scenarios where training data is heavily biased toward low-quality designs.

Effectiveness of Learning the Probabilistic Bridge Model. To demonstrate/ablate the effectiveness of our learning probabilistic bridge model (see Section 3.1.1), we further conducted an experiment that runs gradient ascent on GP posterior mean function for comparison. This simple baseline is denoted as **GA on GP** in Table 1. It is observed that our method significantly outperforms this baseline, confirming the impact of learning probabilistic bridge.

Number of Gradient Steps (M). We experimented with various numbers of gradient steps (M), from the set $\{25, 50, 75, 100\}$ to construct \mathbf{X}_s^- and \mathbf{X}_s^+ during the data generation phase (see Section 3.3). Our experiments reveal that increasing M consistently improves the overall performance of the algorithm as illustrated in Table 6. Increasing the number of gradient steps allows our model to more precisely distinguish between low-value and high-value regions in the distribution, substantially enhancing our performance. However, increasing the number of gradient steps also increases computational time, so we select $M = 100$ as the best balance between performance and efficiency.

Number of Initial (n_p). For each synthetic function generated by the Gaussian process, we will draw a number of initial data points (n_p) from the offline dataset to initiate the exploration into the

low-value and high-value regions via gradient descent and ascent, respectively. We experimented with different numbers of initial points from the set $\{128, 256, 512, 1024\}$. As shown in Table 7, increasing the number of initial points n_p consistently improves performance. This observation is similar to a previous observation that having more well-curated training data tends to enhance the overall model performance. We selected $n_p = 1024$ as the best balance between computational cost and performance score.

Additional Ablation Studies. We further performed a series of ablation studies, examining key hyperparameters of our method, alternative strategies for sampling GP kernel parameters, different data sampling techniques beyond GP, the impact of measurement noise, performance on high-dimensional continuous tasks, and settings with limited query budgets. For completeness, we also report computational complexity analysis and empirical runtime comparisons of **ROOT** against baselines. Due to space constraints, all these results are deferred to Appendices C.

5 Related Works

Existing approaches in offline optimization can be categorized into three main families: **forward modeling, inverse modeling, and learning search policies**.

Forward Modeling tackles out-of-distribution (OOD) issues by penalizing high surrogate predictions on OOD inputs [44, 11, 54, 53, 12, 13, 24, 34, 17, 16]. For example, COM [44] identifies OOD regions early during gradient updates and re-trains the surrogate with regularizers to penalize high-value predictions at these inputs. BOSS[12] introduces a sensitivity-aware regularizer for offline optimizers, while ICT, Tri-mentoring [54, 11] use co-teaching among surrogates to improve performance.

Inverse Modeling avoids OOD problems by directly learning high-value regions [30, 33, 29]. For instance, MIN [30] uses model inversion networks to map scores back to inputs, while ExPT [33] combines unsupervised learning and few-shot experimental design for optimizing synthetic functions. DDOM [29] develops a guided diffusion model to generate designs conditioned on function values. The model is trained using weighted sampling from the offline dataset.

Learning Search Policies aims to replicate optimization paths from low- to high-value designs [28, 8]. BONET [28] synthesizes trajectories from offline data using a heuristic for monotonic transitions and trains an auto-regressive model. PGS [8] reinterprets offline optimization as a reinforcement learning task, which optimizes for an effective policy using sampled trajectories from the offline dataset.

Overall, these methods remain constrained by the availability of offline data. For instance, DDOM [29] employs guided diffusion to learn an inverse mapping from desired performance outputs to potential input designs. However, the adopted diffusion model must be trained on weighted sampling from the offline data, which may lack critical information regarding potential high-performing input regions that are far from the offline regimes.

To address the challenges posed by limited data, we reframe offline optimization as a distributional translation task. This perspective unveils an intriguing direction: rather than depending solely on scarce high-value observations, one can learn a global translation model by stitching together localized transformation examples between low- and high-value regimes. This allows the optimization process to be guided by a learned probabilistic bridge that generalizes across design landscapes, offering a flexible and data-efficient alternative to traditional surrogate-based methods.

6 Conclusion

We proposed a new perspective on offline black-box optimization by reframing it as a distributional translation task between low-value and high-value input regimes. At the core of this approach is the *probabilistic bridge*, a model that learns localized transformation flows conditioned on both source and target designs, and synthesizes them into a global translation mechanism. To address the lack of high-value examples in offline datasets, we introduced a synthetic data generation framework that enables pre-training of a meta probabilistic bridge with strong zero-shot generalization. This shifts the focus from modeling the objective function to modeling design transitions, opening new possibilities for data-efficient optimization. Future directions include exploring alternative bridge parameterizations and extending the framework to more complex optimization settings.

References

- [1] Aria Ahari, Larbi Alili, and Massimiliano Tamborrino. Boundary crossing problems and functional transformations for ornstein–uhlenbeck processes. *Journal of Applied Probability*, 62(1):395–421, 2025.
- [2] Michael Ahn, Henry Zhu, Kristian Hartikainen, Hugo Ponte, Abhishek Gupta, Sergey Levine, and Vikash Kumar. Robel: Robotics benchmarks for learning with low-cost robots. In *Conference on robot learning*, pages 1300–1313. PMLR, 2020.
- [3] Luis A Barrera, Anastasia Vedenko, Jesse V Kurland, Julia M Rogers, Stephen S Gisselbrecht, Elizabeth J Rossin, Jaie Woodard, Luca Mariani, Kian Hong Kock, Sachi Inukai, et al. Survey of variation in human transcription factors reveals prevalent dna binding changes. *Science*, 351(6280):1450–1454, 2016.
- [4] Paul Bogdan, Fan Chen, Aryan Deshwal, Janardhan Rao Doppa, Biresh Kumar Joardar, Hai (Helen) Li, Shahin Nazarian, Linghao Song, and Yao Xiao. Taming extreme heterogeneity via machine learning based design of autonomous manycore systems. In *Proceedings of the International Conference on Hardware/Software Codesign and System Synthesis Companion, CODES+ISSS 2019, part of ESWeek 2019, New York, NY, USA, October 13-18, 2019*, pages 21:1–21:10. ACM, 2019.
- [5] Greg Brockman, Vicki Cheung, Ludwig Pettersson, Jonas Schneider, John Schulman, Jie Tang, and Wojciech Zaremba. Openai gym. *arXiv preprint arXiv:1606.01540*, 2016.
- [6] David Brookes, Hahnbeom Park, and Jennifer Listgarten. Conditioning by adaptive sampling for robust design. In *International conference on machine learning*, pages 773–782. PMLR, 2019.
- [7] Luis Ceze, Mark D. Hill, and Thomas F. Wenisch. Arch2030: A vision of computer architecture research over the next 15 years, 2016.
- [8] Yassine Chemingui, Aryan Deshwal, Trong Nghia Hoang, and Janardhan Rao Doppa. Offline model-based optimization via policy-guided gradient search. In *Proceedings of the AAAI Conference on Artificial Intelligence*, volume 38, pages 11230–11239, 2024.
- [9] Can Chen, Christopher Beckham, Zixuan Liu, Xue Liu, and Christopher Pal. Robust guided diffusion for offline black-box optimization. *Transactions on Machine Learning Research*, 2024.
- [10] Can Chen, Yingxue Zhang, Jie Fu, Xue Liu, and Mark Coates. Bidirectional learning for offline infinite-width model-based optimization. In Alice H. Oh, Alekh Agarwal, Danielle Belgrave, and Kyunghyun Cho, editors, *Advances in Neural Information Processing Systems*, 2022.
- [11] Can Sam Chen, Christopher Beckham, Zixuan Liu, Xue Steve Liu, and Chris Pal. Parallel-mentoring for offline model-based optimization. *Advances in Neural Information Processing Systems*, 36, 2024.
- [12] Manh Cuong Dao, Phi Le Nguyen, Thao Nguyen Truong, and Trong Nghia Hoang. Boosting offline optimizers with surrogate sensitivity. In *Forty-first International Conference on Machine Learning*, 2024.
- [13] Manh Cuong Dao, Phi Le Nguyen, Thao Nguyen Truong, and Trong Nghia Hoang. Incorporating surrogate gradient norm to improve offline optimization techniques. In *The Thirty-eighth Annual Conference on Neural Information Processing Systems*, 2024.
- [14] Aryan Deshwal and Jana Doppa. Combining latent space and structured kernels for Bayesian optimization over combinatorial spaces. *Advances in Neural Information Processing Systems*, 34:8185–8200, 2021.
- [15] Aryan Deshwal, Cory M Simon, and Janardhan Rao Doppa. Bayesian optimization of nanoporous materials. *Molecular Systems Design & Engineering*, 6(12):1066–1086, 2021.

[16] Clara Fannjiang and Jennifer Listgarten. Autofocused oracles for model-based design. *Advances in Neural Information Processing Systems*, 33:12945–12956, 2020.

[17] Justin Fu and Sergey Levine. Offline model-based optimization via normalized maximum likelihood estimation. *arXiv preprint arXiv:2102.07970*, 2021.

[18] Nickolas Gantzler, Aryan Deshwal, Janardhan Rao Doppa, and Cory Simon. Multi-fidelity Bayesian Optimization of Covalent Organic Frameworks for Xenon/Krypton Separations. *Digital Discovery*, 2023.

[19] Wenhao Gao, Sai Pooja Mahajan, Jeremias Sulam, and Jeffrey J Gray. Deep learning in protein structural modeling and design. *Patterns*, 1(9), 2020.

[20] Tuomas Haarnoja, Aurick Zhou, Kristian Hartikainen, George Tucker, Sehoon Ha, Jie Tan, Vikash Kumar, Henry Zhu, Abhishek Gupta, Pieter Abbeel, et al. Soft actor-critic algorithms and applications. *arXiv preprint arXiv:1812.05905*, 2018.

[21] Nikolaus Hansen. The cma evolution strategy: a comparing review. *Towards a new evolutionary computation: Advances in the estimation of distribution algorithms*, pages 75–102.

[22] Jonathan Ho, Ajay Jain, and Pieter Abbeel. Denoising diffusion probabilistic models. *Advances in neural information processing systems*, 33:6840–6851, 2020.

[23] Jonathan Ho and Tim Salimans. Classifier-free diffusion guidance. *arXiv preprint arXiv:2207.12598*, 2022.

[24] Minh Hoang, Azza Fadhel, Aryan Deshwal, Jana Doppa, and Trong Nghia Hoang. Learning surrogates for offline black-box optimization via gradient matching. In *Forty-first International Conference on Machine Learning*, 2024.

[25] Minsu Kim, Federico Berto, Sungsoo Ahn, and Jinkyoo Park. Bootstrapped training of score-conditioned generator for offline design of biological sequences. *arXiv preprint arXiv:2306.03111*, 2023.

[26] Minsu Kim, Jiayao Gu, Ye Yuan, Taeyoung Yun, Zixuan Liu, Yoshua Bengio, and Can Chen. Offline model-based optimization: Comprehensive review. *arXiv preprint arXiv:2503.17286*, 2025.

[27] Ryan Gary Kim, Janardhan Rao Doppa, Partha Pratim Pande, Diana Marculescu, and Radu Marculescu. Machine learning and manycore systems design: A serendipitous symbiosis. *Computer*, 51(7):66–77, 2018.

[28] Siddarth Krishnamoorthy, Satvik Mehul Mashkaria, and Aditya Grover. Generative pretraining for black-box optimization. *arXiv preprint arXiv:2206.10786*, 2022.

[29] Siddarth Krishnamoorthy, Satvik Mehul Mashkaria, and Aditya Grover. Diffusion models for black-box optimization. *arXiv preprint arXiv:2306.07180*, 2023.

[30] Aviral Kumar and Sergey Levine. Model inversion networks for model-based optimization. *Advances in Neural Information Processing Systems*, 33:5126–5137, 2020.

[31] Bo Li, Kaitao Xue, Bin Liu, and Yu-Kun Lai. Bbdm: Image-to-image translation with brownian bridge diffusion models. In *Proceedings of the IEEE/CVF Conference on Computer Vision and Pattern Recognition*, pages 1952–1961, 2023.

[32] Ronny Lorenz, Stephan H. Bernhart, Christoph Höner Zu Siederdissen, Hanna Tafer, Christoph Flamm, Peter F. Stadler, and Ivo L. Hofacker. ViennaRNA Package 2.0. *Algorithms for Molecular Biology*, 6(1):26, November 2011.

[33] Tung Nguyen, Sudhanshu Agrawal, and Aditya Grover. Expt: Synthetic pretraining for few-shot experimental design. *Advances in Neural Information Processing Systems*, 36:45856–45869, 2023.

[34] Han Qi, Yi Su, Aviral Kumar, and Sergey Levine. Data-driven offline decision-making via invariant representation learning. *Advances in Neural Information Processing Systems*, 35:13226–13237, 2022.

[35] Joaquin Quinonero-Candela and Carl Edward Rasmussen. A unifying view of sparse approximate gaussian process regression. *Journal of machine learning research*, 6(Dec):1939–1959, 2005.

[36] C. E. Rasmussen and C. K. I. Williams. *Gaussian Processes for Machine Learning*. MIT Press, 2006.

[37] Samsinai. FLEXS: Fitness landscape exploration sandbox for biological sequence design. <https://github.com/samsinai/FLEXS>, 2023. Accessed: 2025-05-08.

[38] Petra Schneider, W Patrick Walters, Alleyn T Plowright, Norman Sieroka, Jennifer Listgarten, Robert A Goodnow Jr, Jasmin Fisher, Johanna M Jansen, José S Duca, Thomas S Rush, et al. Rethinking drug design in the artificial intelligence era. *Nature Reviews Drug Discovery*, 19(5):353–364, 2020.

[39] Jasper Snoek, L. Hugo, and R. P. Adams. Practical Bayesian optimization of machine learning algorithms. In *Proc. NIPS*, pages 2960–2968, 2012.

[40] Jasper Snoek, Oren Rippel, Kevin Swersky, Ryan Kiros, Nadathur Satish, Narayanan Sundaram, Mostofa Patwary, Mr Prabhat, and Ryan Adams. Scalable bayesian optimization using deep neural networks. In *International conference on machine learning*, pages 2171–2180. PMLR, 2015.

[41] Rong-Xi Tan, Ke Xue, Shen-Huan Lyu, Haopu Shang, yaowang, Yaoyuan Wang, Fu Sheng, and Chao Qian. Offline model-based optimization by learning to rank. In *The Thirteenth International Conference on Learning Representations*, 2025.

[42] Emanuel Todorov, Tom Erez, and Yuval Tassa. Mujoco: A physics engine for model-based control. In *2012 IEEE/RSJ International Conference on Intelligent Robots and Systems*, pages 5026–5033. IEEE, 2012.

[43] Brandon Trabucco, Xinyang Geng, Aviral Kumar, and Sergey Levine. Design-bench: Benchmarks for data-driven offline model-based optimization. In *International Conference on Machine Learning*, pages 21658–21676. PMLR, 2022.

[44] Brandon Trabucco, Aviral Kumar, Xinyang Geng, and Sergey Levine. Conservative objective models for effective offline model-based optimization. In *International Conference on Machine Learning*, pages 10358–10368. PMLR, 2021.

[45] Hanchen Wang, Tianfan Fu, Yuanqi Du, Wenhao Gao, Kexin Huang, Ziming Liu, Payal Chandak, Shengchao Liu, Peter Van Katwyk, Andreea Deac, et al. Scientific discovery in the age of artificial intelligence. *Nature*, 620(7972):47–60, 2023.

[46] Yining Wang, Simon Du, Sivaraman Balakrishnan, and Aarti Singh. Stochastic zeroth-order optimization in high dimensions. In *International conference on artificial intelligence and statistics*, pages 1356–1365. PMLR, 2018.

[47] Z. Wang and S. Jegelka. Max-value entropy search for efficient Bayesian optimization. In *Proc. ICML*, pages 3627–3635, 2017.

[48] Z. Wang, M. Zoghi, F. Hutter, D. Matheson, and N. de Freitas. Bayesian optimization in high dimensions via random embeddings. In *Proc. IJCAI*, pages 1778–1784, 2013.

[49] Z. Wang, M. Zoghi, F. Hutter, D. Matheson, and N. de Freitas. Bayesian optimization in a billion dimensions via random embeddings. *JAIR*, 55:361–387, 2016.

[50] Christopher KI Williams and Carl Edward Rasmussen. *Gaussian processes for machine learning*, volume 2. MIT press Cambridge, MA, 2006.

[51] Ronald J Williams. Simple statistical gradient-following algorithms for connectionist reinforcement learning. *Machine learning*, 8:229–256, 1992.

- [52] Michael S Yao, Yimeng Zeng, Hamsa Bastani, Jacob R. Gardner, James Gee, and Osbert Bastani. Generative adversarial model-based optimization via source critic regularization. In *The Thirty-eighth Annual Conference on Neural Information Processing Systems*, 2024.
- [53] Sihyun Yu, Sungsoo Ahn, Le Song, and Jinwoo Shin. Roma: Robust model adaptation for offline model-based optimization. *Advances in Neural Information Processing Systems*, 34:4619–4631, 2021.
- [54] Ye Yuan, Can Chen, Zixuan Liu, Willie Neiswanger, and Xue Liu. Importance-aware co-teaching for offline model-based optimization. *arXiv preprint arXiv:2309.11600*, 2023.
- [55] Ye Yuan, Youyuan Zhang, Can Chen, Haolun Wu, Melody Zixuan Li, Jianmo Li, James J. Clark, and Xue Liu. Design editing for offline model-based optimization. *Transactions on Machine Learning Research*, 2025.
- [56] Taeyoung Yun, Sujin Yun, Jaewoo Lee, and Jinkyoo Park. Guided trajectory generation with diffusion models for offline model-based optimization. *arXiv preprint arXiv:2407.01624*, 2024.

A Task Details

A.1 Design-Bench Task

Design-Bench [43] is a widely adopted benchmark for evaluating offline black-box optimization algorithms. Table 8 presents the summary of five evaluation tasks in Design-Bench.

Table 8: Overview of tasks in the Design-Bench benchmark. The ground-truth oracle functions for these tasks (unknown to our algorithm) are accessible during evaluation.

Task	Offline Size	Input Dimension	Input Category	Input Type	Oracle
TF Bind 8	32,898	8	4	Discrete	Exact
TF Bind 10	10,000	10	4	Discrete	Exact
Ant Morphology	10,004	60	N/A	Continuous	Exact
D'Kitty Morphology	10,004	56	N/A	Continuous	Exact
RNA-Binding	5000	14	4	Discrete	Exact

TF Bind 8 and TF Bind 10: DNA Sequence Optimization. The goals of the **TF Bind 8** and **TF Bind 10** tasks are to discover, respectively, the length-8 and length-10 DNA sequences with the strongest binding affinity to a specific transcription factor (SIX6_REF_R1 by default) [3]. In these settings, each DNA candidate is a sequence of nucleotides where each nucleotide has 4 possible categorical values. The Design-Bench benchmark grants access to the full oracle functions for the **TF-Bind-8** and **TF-Bind-10** tasks, which correspond to databases containing exact binding affinities for all possible sequences (i.e., 4^8 and 4^{10} combinations, respectively). Following the evaluation protocol in [43], a fixed subset of sequences is sampled from each oracle and used as the offline dataset for all baselines. In particular, **TF-Bind-8** provides an offline dataset of 32,898 sequences while **TF-Bind-10** provides an offline dataset with 10,000 sequences.

Ant and D'Kitty Morphology: Robot Morphology Optimization. These tasks focus on optimizing the physical structure of two simulated robots: (1) Ant from OpenAI Gym [5] and (2) D'Kitty from ROBEL [2]. In **Ant Morphology**, the objective is to find the structure of a quadruped robot to maximize its running speed. In **D'Kitty Morphology** the goal is to find the most effective structure for the D'Kitty robot that enables it to reach a specific target. In particular, each structure candidate specifies the morphology parameters, such as the size, orientation, and placement of limbs, for a robot controller which will be trained using the Soft Actor-Critic algorithm [20]. For the Ant robots, there are 60 morphology parameters. For the D'Kitty robots, there are 56 morphology parameters. The solution quality of each structure candidate is obtained by simulating the corresponding trained controller in the MuJoCo [42] environment. Each simulation runs for 100 steps and the overall solution quality is obtained by averaging simulation results across 16 independent runs.

A.2 RNA Task

RNA-Binding [32]. This is an inverse-folding task whose objective is to optimize RNA sequences of fixed length (14 nucleotides) over the alphabet {A, U, C, G}, which are abbreviations for adenine, uracil, cytosine, and guanine, respectively. In particular, the task is to find a sequence whose predicted minimum-free-energy (MFE) structure maximizes its binding affinity to a given transcription factor. We follow the benchmark setup of Bootgen [25] by considering three target structures **RNA-A** (L14 RNA1), **RNA-B** (L14 RNA2), and **RNA-C** (L14 RNA3). To construct the offline dataset D_o , we use the FLEXS codebase [37] to generate sequences uniformly at random. The RNAinverse algorithm from ViennaRNA 2.0 is then applied iteratively until 5,000 sequences with minimum free energy (MFE) below 0.12 are obtained, forming the final offline dataset.

B Detailed Algorithmic Description and Implementation of ROOT

B.1 Generating Synthetic Data with GP

To generate a diverse range of synthetic functions which are sufficiently similar to the oracle, we first sample the kernel parameters ℓ_s (lengthscale) and σ_s^2 (variance) uniformly from the ranges $[\ell_0 - \delta, \ell_0 + \delta]$ and $[\sigma_0^2 - \delta, \sigma_0^2 + \delta]$, where ℓ_0 , σ_0^2 and δ are fixed initial hyperparameters, as reported

Table 9: Hyperparameters for the synthetic data generation of **ROOT**.

Hyperparameter	Value
ℓ_0, σ_0^2	1.0 (continuous) 6.25 (discrete)
δ	0.25
Step size (η)	0.001 (continuous) 0.05 (discrete)
Number of gradient steps (M)	100
Threshold (τ)	0.001

Algorithm 1 Synthetic Data Generation via Simulating Gaussian Process (GP) Posteriors

- 1: **Input:** Offline dataset $D_o = \{\mathbf{x}_i, y_i\}_{i=1}^n$, number of functions per epoch n_e , number of points per function n_p , number of gradient steps M
- 2: **Output:** Synthetic dataset $D_s = \{(\mathbf{X}^-, \mathbf{y}^-), (\mathbf{X}^+, \mathbf{y}^+)\}$
- 3: $\mathcal{D}_s \leftarrow \emptyset$
- 4: **for** $s = 1$ **to** n_e **do**
- 5: Sample kernel parameters $\phi_s = (\ell_s, \sigma_s^2)$: $\ell_s \sim U(\ell_0 - \delta, \ell_0 + \delta)$, $\sigma_s^2 \sim U(\sigma_0^2 - \delta, \sigma_0^2 + \delta)$
- 6: Compute the mean function \bar{g}_{ϕ_s} of the posterior Gaussian process via Eq. 11
- 7: Sample a subset of n_p points from offline data: $\mathcal{D}_0 \subset D_o$ where $|\mathcal{D}_0| = n_p$
- 8: Compute the set of low-value designs \mathbf{X}_s^- using Eq. 12
- 9: Compute the set of high-value designs \mathbf{X}_s^+ using Eq. 13
- 10: Compute corresponding low and high scores: $\mathbf{y}_s^- = \bar{g}_{\phi_s}(\mathbf{X}_s^-)$, $\mathbf{y}_s^+ = \bar{g}_{\phi_s}(\mathbf{X}_s^+)$
- 11: $D_s \leftarrow D_s \cup \{(\mathbf{X}_s^-, \mathbf{y}_s^-), (\mathbf{X}_s^+, \mathbf{y}_s^+)\}$
- 12: **end for**
- 13: **Return** D_s

in Table 9. After sampling, we compute the mean function of the Gaussian process posterior based on the offline data. We then sample n_p points from the offline data and perform $M = 100$ gradient ascent and gradient descent steps with a step size η (more details are provided in Section 3.3). To enhance the quality of our synthetic data, we filter out any pair of low- and high-value points $(\mathbf{x}^-, \mathbf{y}^-)$ and $(\mathbf{x}^+, \mathbf{y}^+)$ whose difference between \mathbf{y}^+ and \mathbf{y}^- is smaller than a threshold τ . All key hyperparameters for this process are listed in Table 9. The pseudocode of the algorithm is presented in Algorithm 1.

B.2 Learning the Probabilistic Bridge Model

This section provides further details regarding the implementation of the learning loss in Eq. 8 with respect to its Brownian bridge instantiation in Section 3.2. In particular, following the formulation of $q(\mathbf{x}_t \mid \mathbf{x}_0, \mathbf{x}_T)$ in Eq. 10, we can express \mathbf{x}_t

$$\mathbf{x}_t = \left(1 - \frac{t}{T}\right) \mathbf{x}_0 + \frac{t}{T} \mathbf{x}_T + \sqrt{\kappa_{t,t}} \boldsymbol{\epsilon} \quad (15)$$

where $\boldsymbol{\epsilon}_t \sim \mathbb{N}(0, \mathbf{I})$ and $\kappa_{t,t} = 2(m_t - m_t^2)$ with $m_t = t/T$. This reproduces the Brownian Bridge Diffusion Model [31]. Following the derivation in [31], we obtain:

$$q(\mathbf{x}_{t-1} \mid \mathbf{x}_t, \mathbf{x}_0, \mathbf{x}_T) = \mathbb{N}(\boldsymbol{\mu}(\mathbf{x}_t, \mathbf{x}_0, \mathbf{x}_T), \tilde{\kappa}_{t-1} \cdot \mathbf{I}),$$

where the mean is

$$\boldsymbol{\mu}(\mathbf{x}_t, \mathbf{x}_0, \mathbf{x}_T) = u_t \cdot \mathbf{x}_t + v_t \cdot \mathbf{x}_T + w_t \cdot (m_t(\mathbf{x}_T - \mathbf{x}_0) + \sqrt{\kappa_{t,t}} \boldsymbol{\epsilon}), \quad (16)$$

and the variance is

$$\tilde{\kappa}_{t-1} = \left(\kappa_{t,t} - \kappa_{t-1,t-1} \cdot \frac{(1 - m_t)^2}{(1 - m_{t-1})^2} \right) \cdot \frac{\kappa_{t-1,t-1}}{\kappa_{t,t}}. \quad (17)$$

Algorithm 2 Learning the Probabilistic Bridge and Simulation for Offline Optimization (**ROOT**)

1: **Input:** Offline dataset $D_o = \{\mathbf{x}_i, y_i\}_{i=1}^n$, number of epochs E , number of diffusion steps T , scale α , best objective value y_* , conditional dropout probability ρ , number of iterations I
2: **Output:** High-value candidate \mathbf{x}_0^*
3:
4: **Learning Probabilistic Bridge Phase:**
5: Initialize model parameters θ
6: **for** $e = 1$ **to** E **do**
7: Generate synthetic dataset D_s from Algorithm 1
8: **for** $i = 1$ **to** I **do**
9: Sample $\{\mathbf{x}_T, y_T, \mathbf{x}_0, y_0\} \sim \mathcal{D}_s = \{\mathbf{X}^-, \mathbf{y}^-, \mathbf{X}^+, \mathbf{y}^+\}$
10: Sample timestep $t \sim \text{Uniform}(1, T)$, $\gamma \sim \text{Ber}(\rho)$, $y = [y_T, y_0]$
11: Forward diffusion: $\mathbf{x}_t = (1 - m_t) \cdot \mathbf{x}_0 + m_t \cdot \mathbf{x}_T + \sqrt{\kappa_{t,t}} \boldsymbol{\epsilon}$ where $\boldsymbol{\epsilon} \sim \mathcal{N}(0, \mathbf{I})$
12: Gradient descent step: $\nabla_{\theta} \|m_t(\mathbf{x}_T - \mathbf{x}_0) + \sqrt{\kappa_{t,t}} \boldsymbol{\epsilon} - \boldsymbol{\epsilon}_{\theta}(\mathbf{x}_t, t, (1 - \gamma) \cdot y + \gamma \cdot \emptyset)\|^2$ (Eq. 24)
13: **end for**
14: **end for**
15:
16: **Simulation Phase:**
17: $\{\mathbf{x}_T, y_T\} \leftarrow 128$ best designs in D_o , $y = [y_T, \alpha \cdot y_*]$
18: **for** $t = T$ **to** 1 **do**
19: $\mathbf{z} \sim \mathcal{N}(0, \mathbf{I})$ if $t > 0$ else $\mathbf{z} = 0$
20: Compute $\boldsymbol{\epsilon}_{\theta}(\mathbf{x}_t, t, y)$ via Eq. 25
21: $\mathbf{x}_{t-1} = u_t \cdot \mathbf{x}_t + v_t \cdot \mathbf{x}_T + w_t \cdot \boldsymbol{\epsilon}_{\theta}(\mathbf{x}_t, t, y) + \sqrt{\tilde{\kappa}_{t-1}} \cdot \mathbf{z}$
22: **end for**
23:
24: **Return:** high-value design $\mathbf{x}_0^* = \mathbf{x}_0$

Furthermore, the coefficients for the above mean function were derived as

$$u_t = \frac{\kappa_{t-1,t-1}}{\kappa_{t,t}} \cdot \frac{1 - m_t}{1 - m_{t-1}} + \frac{\kappa_{t,t} - \kappa_{t-1,t-1} \cdot \frac{(1-m_t)^2}{(1-m_{t-1})^2}}{\kappa_{t,t}} \cdot (1 - m_{t-1}), \quad (18)$$

$$v_t = m_{t-1} - m_t \cdot \frac{1 - m_t}{1 - m_{t-1}} \cdot \frac{\kappa_{t-1,t-1}}{\kappa_{t,t}}, \quad (19)$$

$$w_t = (1 - m_{t-1}) \cdot \frac{\kappa_{t,t} - \kappa_{t-1,t-1} \cdot \frac{(1-m_t)^2}{(1-m_{t-1})^2}}{\kappa_{t,t}}. \quad (20)$$

This setup thus provides training examples of localized flows which can be used to learn a parameterized target-agnostic transformation that maps from a source \mathbf{x}_T to a plausible target \mathbf{x}_0 without knowing it beforehand using the loss in Eq. 8. To implement this loss, we parameterize the transition probability of the aforementioned target-agnostic transformation $p_{\theta}(\mathbf{x}_{t-1}|\mathbf{x}_t, \mathbf{x}_T)$ as:

$$p_{\theta}(\mathbf{x}_{t-1}|\mathbf{x}_t, \mathbf{x}_T) = \mathcal{N}\left(\mathbf{x}_{t-1}; \boldsymbol{\mu}_{\theta}(\mathbf{x}_t, \mathbf{x}_T, t), \tilde{\kappa}_{t-1} \cdot \mathbf{I}\right), \quad (21)$$

where the $\boldsymbol{\mu}_{\theta}$ is parameterized following Eq. 16:

$$\boldsymbol{\mu}_{\theta}(\mathbf{x}_t, \mathbf{x}_T, t) = u_t \cdot \mathbf{x}_t + v_t \cdot \mathbf{x}_T + w_t \cdot \boldsymbol{\epsilon}_{\theta}(\mathbf{x}_t, t), \quad (22)$$

which features a parameterized noise prediction network $\boldsymbol{\epsilon}(\mathbf{x}_t, t)$ to predict the noise perturbed quantity $m_t(\mathbf{x}_T - \mathbf{x}_0) + \sqrt{\kappa_{t,t}} \boldsymbol{\epsilon}$ of a local flow at time t . Under this parameterization, the training loss in Eq. 8 can be simplified as,

$$\boldsymbol{\theta}_{\text{PB}} = \arg \min_{\theta} \mathbb{E}_{\mathbf{x}_0, \mathbf{x}_T, \boldsymbol{\epsilon}} \left[\|m_t(\mathbf{x}_T - \mathbf{x}_0) + \sqrt{\kappa_{t,t}} \boldsymbol{\epsilon} - \boldsymbol{\epsilon}_{\theta}(\mathbf{x}_t, t)\|^2 \right]. \quad (23)$$

It is then approximately optimized via sampling $(\mathbf{x}_T, \mathbf{x}_0)$ from the synthetic dataset D_s created using Algorithm 1 above. For a more practical implementation, we further leverage the corresponding scores y_T and y_0 of \mathbf{x}_T and \mathbf{x}_0 which are also included in D_s . In particular, we further parameterize $\boldsymbol{\epsilon}_{\theta}(\mathbf{x}_t, t)$ as $\boldsymbol{\epsilon}_{\theta}(\mathbf{x}_t, t, (1 - \gamma)y + \gamma\emptyset)$ with $y = (y_0, y_T)$ and $\gamma \sim \text{Ber}(\rho)$ following similar practice

in guided diffusion [23]. The intuition is that we want to leverage the output scores to guide the noise prediction network but at the same time, we do not want the network to overly depend on such guidance. This is enforced using the dropout trick which randomly removes the guiding information during training with probability $\rho \in (0, 1)$. The above learning loss can then be recast as:

$$\boldsymbol{\theta}_{\text{PB}}^* \triangleq \arg \min_{\boldsymbol{\theta}} \mathbb{E}_{\mathbf{x}_0, y_0, \mathbf{x}_T, y_T, \boldsymbol{\epsilon}} \left[\|m_t(\mathbf{x}_T - \mathbf{x}_0) + \sqrt{\kappa_{t,t}} \boldsymbol{\epsilon} - \boldsymbol{\epsilon}_{\boldsymbol{\theta}}(\mathbf{x}_t, t, (1 - \gamma) \cdot y + \gamma \cdot \emptyset)\|^2 \right], \quad (24)$$

where $\gamma \sim \text{Ber}(\rho)$. Once trained, the noise network $\boldsymbol{\epsilon}_{\boldsymbol{\theta}}$ is used as below during the simulation phase:

$$\boldsymbol{\epsilon}_{\boldsymbol{\theta}}(\mathbf{x}_t, t, y) = (1 + \beta) \cdot \boldsymbol{\epsilon}_{\boldsymbol{\theta}}(\mathbf{x}_t, t, y) - \beta \cdot \boldsymbol{\epsilon}_{\boldsymbol{\theta}}(\mathbf{x}_t, t, \emptyset), \quad (25)$$

where β is the classifier free guidance weight and $y = [y_T, \alpha \cdot y_*]$ with y_* denotes the maximum oracle score. Our detail algorithm is presented in Algorithm 2.

For more details, we utilize an MLP $\boldsymbol{\epsilon}_{\boldsymbol{\theta}}(\mathbf{x}_t, t, y)$ comprising four layers, each with 1024 units. Each layer employs the Swish activation function, $\text{Swish}(z) = z\sigma(z)$, where $\sigma(z)$ denotes the sigmoid function. The MLP is trained using the Adam optimizer for 100 epochs with a learning rate of 0.001. During each epoch, we sample $n_e = 8$ synthetic functions from the Gaussian process (the total number of synthetic functions is $n_g = n_e \times E = 8 \times 100 = 800$ functions) and generate $n_p = 1024$ samples for each function. At the testing phase, we sample high-value design candidates from the 128 best designs in the offline dataset, using $T = 200$ sequential denoising steps. All hyperparameters for modeling, training, and sampling with our model are summarized in Table 10.

Table 10: Hyperparameters for the generalized Brownian Bridge diffusion process in **ROOT**.

	Hyperparameter	Value
Architecture	Hidden size	1024
	Number of layers	4
	Activation	Swish
Training	Number of epochs (E)	100
	Number of functions (n_e) (per epoch)	8
	Number of data points (n_p) (per function)	1024
	Learning rate	0.001
	Optimizer	Adam
	Batch size	64
	Conditional dropout (ρ)	0.15
Sampling	α	0.8
	β	-1.5
	Denoising steps	200

For reproducibility, our implementation is made available at the following anonymous link: <https://anonymous.4open.science/r/ROOT>

C Additional Experiment Results

C.1 Computation Resource

All our experiments were conducted on a system with the following specifications: Ubuntu 20.04.5, a single NVIDIA A100-SXM4-80GB GPU, and CUDA 10.1. Notably, our method requires less than 6GB of GPU memory per run.

C.2 Additional Performance Evaluation of ROOT

In the main text, we have reported the 100th percentile scores. In this section, we present additional evaluation results at 80th and 50th percentiles, providing further insights into the performance distribution of our **ROOT**.

C.2.1 Performance Evaluation at 80th Percentile

As shown in Table 11, our method **ROOT** consistently demonstrates strong performance at the 80th percentile level, achieving the best mean rank, i.e., **1.5**. Notably, in the **Ant** and **D' Kitty** tasks,

ROOT achieves significant improvements over all baselines with remarkable score differences of **0.098** and **0.025** over the runner-ups in those tasks, respectively. **ROOT** also achieves best result in **TF-Bind-8**, outperforming the runner-up with a margin of **0.011**. In the **TF-Bind-10**, **ROOT** performs competitively to the best baselines. Overall, these results demonstrate the consistent reliability and stability of our model’s performance.

Table 11: Experiments on Design-Bench Tasks. We report 80th percentile score among $Q = 128$ candidates. **Blue** denotes the best entry in the column, and **Brown** denotes the second best. **Mean Rank** means the average rank of the method over all the experiment benchmarks.

Method	Benchmarks				Mean Rank
	Ant	D’Kitty	TFBind8	TFBind10	
D_o (best)	0.565	0.884	0.439	0.467	-
BO-qEI	0.629 ± 0.000	0.884 ± 0.000	0.439 ± 0.000	0.510 ± 0.011	11.00 / 15
CMA-ES	0.007 ± 0.013	0.718 ± 0.001	0.652 ± 0.017	0.543 ± 0.013	9.50 / 15
REINFORCE	0.182 ± 0.017	0.562 ± 0.197	0.622 ± 0.030	0.519 ± 0.007	11.25 / 15
GA	0.189 ± 0.014	0.762 ± 0.036	0.828 ± 0.027	0.516 ± 0.004	8.75 / 15
COMs	0.635 ± 0.031	0.887 ± 0.004	0.738 ± 0.027	0.526 ± 0.012	5.25 / 15
CbAS	0.542 ± 0.034	0.813 ± 0.012	0.585 ± 0.030	0.517 ± 0.008	10.25 / 15
MINs	0.746 ± 0.011	0.908 ± 0.004	0.545 ± 0.031	0.519 ± 0.010	6.50 / 15
RoMA	0.298 ± 0.033	0.738 ± 0.018	0.661 ± 0.010	0.525 ± 0.003	9.00 / 15
DDOM	0.749 ± 0.029	0.865 ± 0.009	0.526 ± 0.017	0.506 ± 0.004	9.75 / 15
ICT	0.708 ± 0.019	0.898 ± 0.004	0.667 ± 0.035	0.525 ± 0.016	6.00 / 15
Tri-mentoring	0.722 ± 0.015	0.902 ± 0.003	0.683 ± 0.047	0.531 ± 0.007	4.00 ± 0.15
GTG	0.725 ± 0.077	0.913 ± 0.007	0.611 ± 0.038	0.506 ± 0.006	7.75 / 15
LTR	0.679 ± 0.016	0.902 ± 0.002	0.734 ± 0.025	0.508 ± 0.010	7.00 / 15
GABO	0.016 ± 0.009	0.705 ± 0.002	0.676 ± 0.021	0.512 ± 0.008	11.25 / 15
ROOT (ours)	0.847 ± 0.005	0.938 ± 0.002	0.839 ± 0.015	0.526 ± 0.007	1.50 ± 0.15

C.2.2 Performance Evaluation at 50th Percentile

Table 12 reports the results achieved by all baselines at 50-th percentile. Consistent to or earlier observations, **ROOT** again achieves the best mean rank of **2.0**. In particular, we surpass the runner-up baseline, Gradient Ascent (GA), in the **TF-Bind-8** task with a significant score difference of **0.072**, securing the top rank among all other methods. In the **Ant** and **D’Kitty** tasks, **ROOT** also achieves substantial score gaps of **0.067** and **0.018** over the corresponding runner-ups, respectively. Furthermore, the reported standard deviations of **ROOT** in those tasks are **0.014** and **0.003** which are much lower than those of other baselines. This further ascertains the stability and superior performance of our method across the evaluation benchmark.

C.3 Score Distribution of ROOT

To provide a more holistic comparison between the score distribution of **ROOT** and those of others, we collect the design candidates obtained from 8 runs ($128 \times 8 = 1024$ designs) to plot the distribution of scores achieved by **ROOT** and several other representative baselines. The results are shown in Fig. 2. Due to the wide range of scores produced by CMA-ES on the **Ant** task, we separately plot and compare its score distribution against **ROOT**. The remaining plots visualize and compare the score distributions of **ROOT** and 5 representative baselines. In each plot, we annotate the max and median lines to ease the visual comparison. In particular, Fig. 2 reveals that **ROOT** often has a score distribution skewed towards higher-value regions, especially in the **D’Kitty** task. In the **Ant** task, although **ROOT**’s max score is not as high as that of CMA-ES, CMA-ES only produces a single good design while the rest (in its solution set) perform poorly, as also observed in Table 11 and Table 12. Otherwise, it can be observed consistently across all plots **ROOT** achieves better score distributions compared to other baselines.

Summary. In conclusion, all reported results have demonstrated consistently that our proposed method **ROOT** is, on average, the best-performing baseline in both score distributions and targeted

Table 12: Experiments on Design-Bench Tasks. We report 50th percentile score among $Q = 128$ candidates. **Blue** denotes the best entry in the column, and **Brown** denotes the second best. **Mean Rank** means the average rank of the method over all the experiment benchmarks.

Method	Benchmarks				Mean Rank
	Ant	D'Kitty	TFBind8	TFBind10	
D_o (best)	0.565	0.884	0.439	0.467	-
BO-qEI	0.569 \pm 0.000	0.883 \pm 0.000	0.439 \pm 0.000	0.469 \pm 0.005	7.75 / 15
CMA-ES	-0.043 \pm 0.007	0.674 \pm 0.016	0.536 \pm 0.012	0.490 \pm 0.015	8.75 / 15
REINFORCE	0.140 \pm 0.026	0.510 \pm 0.203	0.450 \pm 0.024	0.470 \pm 0.010	11.00 / 15
GA	0.137 \pm 0.014	0.591 \pm 0.132	0.603 \pm 0.045	0.469 \pm 0.006	8.75 / 15
COMs	0.471 \pm 0.034	0.862 \pm 0.003	0.598 \pm 0.031	0.475 \pm 0.010	5.75 / 15
CbAS	0.369 \pm 0.008	0.748 \pm 0.016	0.441 \pm 0.021	0.465 \pm 0.006	10.75 / 15
MINs	0.618 \pm 0.016	0.889 \pm 0.003	0.421 \pm 0.017	0.467 \pm 0.010	7.25 / 15
RoMA	0.224 \pm 0.020	0.545 \pm 0.170	0.519 \pm 0.073	0.518 \pm 0.003	8.50 / 15
DDOM	0.568 \pm 0.066	0.814 \pm 0.016	0.404 \pm 0.012	0.456 \pm 0.002	11.00 / 15
ICT	0.554 \pm 0.018	0.872 \pm 0.007	0.557 \pm 0.031	0.457 \pm 0.033	8.25 / 15
Tri-mentoring	0.572 \pm 0.016	0.884 \pm 0.001	0.562 \pm 0.051	0.475 \pm 0.009	4.25 / 15
GTG	0.645 \pm 0.098	0.901 \pm 0.005	0.460 \pm 0.032	0.452 \pm 0.010	7.25 / 15
LTR	0.568 \pm 0.016	0.885 \pm 0.002	0.566 \pm 0.026	0.466 \pm 0.011	6.00 / 15
GABO	-0.039 \pm 0.004	0.674 \pm 0.005	0.496 \pm 0.011	0.457 \pm 0.008	11.50 / 15
ROOT (ours)	0.712 \pm 0.014	0.919 \pm 0.003	0.675 \pm 0.026	0.473 \pm 0.004	2.00 / 15

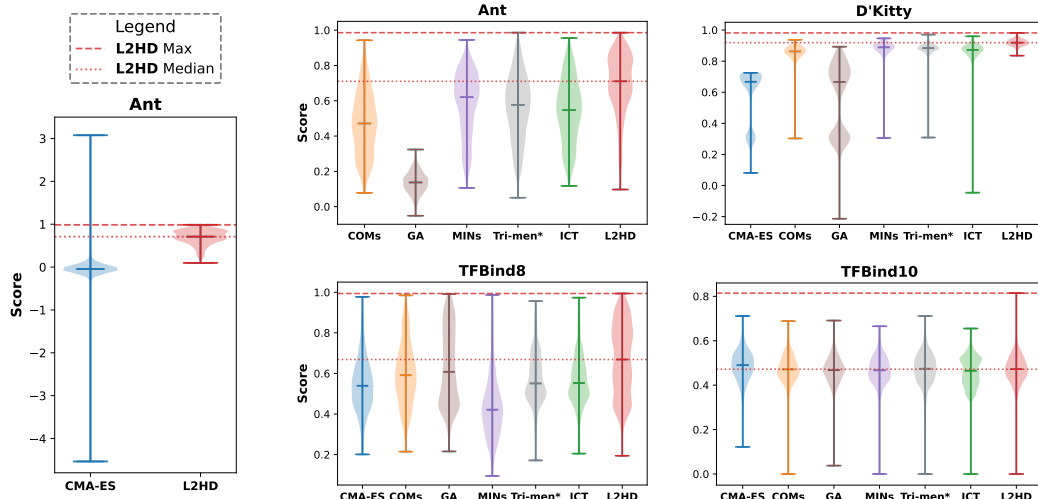


Figure 2: Score distribution of found candidates of **ROOT** compared to others. To avoid cluttering the plots with long chunks of text, we use the abbreviation **Tri-men*** to denote **Tri-mentoring**.

evaluation percentiles. This consistent performance not only highlights the effectiveness and stability of **ROOT** but also reaffirms the robustness of our approach across a wide-range of tasks.

C.4 Computational Complexity Analysis

Computational Complexity. Computational cost of **ROOT** is as follows:

- For each training epoch: Fitting n_f Gaussian processes requires $O(n_f n^3)$ where n is the offline data size. Performing M gradient steps (querying the GP’s mean function) to generate n_p synthetic points from each of n_f functions requires $O(n_f M n_p n)$. Training the BBDM model requires T diffusion steps per sample, where each step involves a forward and backward pass through the score

network ϵ_θ , giving a total cost of $O(T(f_\theta + b_\theta)n_f n_p)$, where f_θ, b_θ denote the cost of forward and backward, respectively.

- For the whole training process, the overall cost is $O(E(n_f n^3 + n_f M n_p n + T(f_\theta + b_\theta)n_f n_p))$ where E is the number of epochs.
- For the inference process, the overall cost is $O(QDf_\theta)$ where Q and D are the number of selected candidates and denoising steps.

Therefore, the total computational cost of **ROOT** is:

$$O(E(n_f n^3 + n_f M n_p n + T(f_\theta + b_\theta)n_f n_p)) + O(QDf_\theta)$$

Furthermore, we note that the most complexity term in **ROOT**’s computational cost, GP fitting, can be further mitigated by using sparse GP techniques [35], which scales linearly in the number of inputs.

Empirical Runtime. We empirically evaluate the runtime of our method and compare it against several baselines across a range of tasks. As shown in Table 13, the results demonstrate that **ROOT** achieves faster execution time than several widely used baselines, including CMA-ES, MINS, and Tri-mentoring, while maintaining competitive or superior performance. All experiments are conducted on a **single GPU**, with each task requiring approximately **4GB** of memory.

Table 13: Runtime (in seconds) of different models across four tasks.

Model	Ant	D’Kitty	TF-Bind-8	TF-Bind-10
GA	122	200	124	420
BO-QEI	219	310	402	383
CMA-ES	5747	4889	2667	4323
MINS	797	998	2213	792
REINFORCE	240	257	507	373
CBAS	394	390	835	529
ICT	188	189	216	639
Tri-mentoring	4276	3921	4673	3410
DEMO	668	1489	1024	1696
ROOT	298	297	407	575

C.5 Effectiveness of Gaussian process for Generating Synthetic Data.

C.5.1 DNN-based Approach for Generating Synthetic Data

There are several strategies for sampling closed-form functions fitted to offline data (to provide functions which are similar to the oracle). In **ROOT**, we adopt a standard Gaussian process (GP) approach due to its efficiency, ease of implementation, and strong empirical performance. GPs are particularly advantageous for their simplicity in debugging and their effectiveness in modeling predictive uncertainty. Our motivation is further motivated by ExPT [33], a recent few-shot offline optimization baseline, which similarly employs GPs to generate pseudo labels for offline data.

While alternative generative models exist, they often introduce additional complexity and computational overhead. For instance, we conducted experiments using deep neural networks (DNNs) in place of GPs. One such approach involves randomly initializing the weights of a DNN and training it to fit the offline dataset, then serving as a single sampled function. However, this approach is computationally expensive. Generating 800 such functions using DNNs, each requiring 800 separate training runs, takes approximately **100** minutes, compared to under **300** seconds for the entire training process using our GP-based method.

To further investigate this, we evaluated two less costly alternative setups: (1) an ensemble of five DNNs replacing all 800 GP functions, denoted as **DNN5**, and (2) a single DNN replacing all 800 GP sampled functions, denoted as **DNN1**. As shown in the Table 14, both alternatives perform worse than our GP-based approach and incur significantly higher computational costs.

Table 14: Performance and runtime of different methods for sampling function on the **Ant** task.

Model	Performance	Time (s)
DNN5	0.637 ± 0.268	1297
DNN1	0.630 ± 0.201	751
ROOT	0.965 ± 0.014	298

C.5.2 Bins-based Approach for Generating Synthetic Data

Beyond the DNN-based approach, we also explore two other heuristic methods that do not depend on Gaussian processes (GP). The first method, *2 bins*, partitions the offline data into two bins, the lowest 50th percentile and the highest 50th percentile, and sample low- and high-value designs (\mathbf{X}^- , \mathbf{X}^+) from the corresponding bins respectively. The second method, *64 bins*, divides the data into 64 bins based on the y values and then sample \mathbf{X}^- from the lowest bin and \mathbf{X}^+ from the highest. This approach is similar to the sampling strategy in [28], where trajectories with increasing outputs are selected from offline data to train a model that progressively guides designs from the lowest to the highest bin. In addition, we also examine another GP-based approach that utilizes only one GP function to generate synthetic data. As reported in Table 15, the GP-based methods consistently outperform the above bin-based heuristic approaches, with GP (800 functions) achieving the best performance.

Table 15: Effectiveness of Gaussian process for generating synthetic data.

	Type	Ant	D'Kitty	TF-Bind-8	TF-Bind-10
No-GP	2 bins	0.745 ± 0.097	0.952 ± 0.007	0.775 ± 0.057	0.641 ± 0.034
	64 bins	0.941 ± 0.020	0.952 ± 0.009	0.837 ± 0.055	0.651 ± 0.054
GP	GP (1 function)	0.955 ± 0.013	0.971 ± 0.004	0.984 ± 0.012	0.657 ± 0.029
	GP (800 functions)	0.965 ± 0.014	0.972 ± 0.005	0.986 ± 0.007	0.685 ± 0.053

C.6 GP Hyperparameters Sampling Methods

To diversify the GP mean functions, various approaches can be used to sample GP hyperparameters. In our work, we adopt a simple strategy by uniformly sampling the GP hyperparameters, i.e., the lengthscale ℓ_s and variance σ_s , from a fixed range, as presented in line 5 of Algorithm 1. This approach follows the prior practice in ExPT [33], which also samples these hyperparameters uniformly from a small range and achieves strong performance.

To explore alternative strategies, we have conducted additional experiments. In a **MAP-based** setting, we first optimize the hyperparameters ℓ_0 and σ_0 by minimizing the negative log marginal likelihood (NLML) on $D_o = \{\mathbf{x}_i, y_i\}_{i=1}^n$, which is commonly used in Gaussian processes:

$$\mathcal{L}_{\text{NLML}}(\phi) = \frac{1}{2} \mathbf{y}^\top K_\phi^{-1} \mathbf{y} + \frac{1}{2} \log |K_\phi| + \frac{n}{2} \log 2\pi,$$

where K_ϕ is the kernel matrix parameterized by $\phi = \{\ell_0, \sigma_0\}$, and n is the number of training data points. After obtaining these MAP estimates, we sample new hyperparameters uniformly around them: $\ell_s \sim [\ell_0 - \delta, \ell_0 + \delta]$ and $\sigma_s \sim [\sigma_0 - \delta, \sigma_0 + \delta]$, instead of setting ℓ_0, σ_0 as in Table 9.

In addition, we have also experimented with an **MCMC-based** approach to sample these hyperparameters. In this setting, we first define a prior distribution $p(\ell_s, \sigma_s)$ (e.g., a Gaussian prior) and a likelihood $p(D_o \mid \ell_s, \sigma_s)$, derived similarly from the marginal likelihood. We then apply MCMC sampling to draw n_g hyperparameter combinations from the posterior distribution, i.e. $p(\ell_s, \sigma_s \mid D_o) \propto p(D_o \mid \ell_s, \sigma_s) \times p(\ell_s, \sigma_s)$.

As shown in Table 16, our uniform sampling method consistently outperforms the aforementioned alternatives. Also, both alternatives introduce significant computational overhead. In particular, the MCMC-based approach requires substantial runtime, incurring approximately **1000** seconds per run, even when using only 8 warmup steps. We leave further exploration of more sophisticated hyperparameter sampling strategies to future work.

Table 16: Performance and runtime of different GP hyperparameter sampling methods on **Ant** task.

Method	Performance
MAP ($n_g = 800$)	0.940 ± 0.023
MCMC ($n_g = 200$)	0.884 ± 0.017
MCMC ($n_g = 400$)	0.921 ± 0.010
MCMC ($n_g = 600$)	0.932 ± 0.016
MCMC ($n_g = 800$)	0.916 ± 0.009
ROOT ($n_g = 800$)	0.965 ± 0.014

C.7 Hyper-parameter Tuning

Number of GP mean functions. We additionally conducted experiments on the number of GP mean functions to generate synthetic data. In our original method, we use $n_g = n_e \times M = 800$ functions; here, we vary this number from 100 to 1000. The empirical results in Table 17 indicate that the final performance improves as the number of Gaussian Processes (GPs) increases. However, there may exist a saturation point (e.g., 800 GPs), beyond which further increasing the number of GPs could lead to a decline in performance.

Table 17: Performance on **Ant** and **TF-Bind-10** with varying number of GPs.

#GPs	Ant	TF-Bind-10
100	0.914 ± 0.015	0.632 ± 0.020
200	0.914 ± 0.015	0.677 ± 0.038
400	0.959 ± 0.010	0.631 ± 0.018
600	0.956 ± 0.021	0.674 ± 0.044
800 (ROOT)	0.965 ± 0.014	0.685 ± 0.053
1000	0.960 ± 0.016	0.662 ± 0.033

GP hyperparameters. We also employed an ablation study to see the effect of Gaussian hyperparameters (i.e., initial lengthscale ℓ_0) on our final results. As can be seen clearly from the Fig. 3, the optimal range for ℓ_0 yields around 1.0 for the continuous tasks and 6.25 for the discrete tasks.

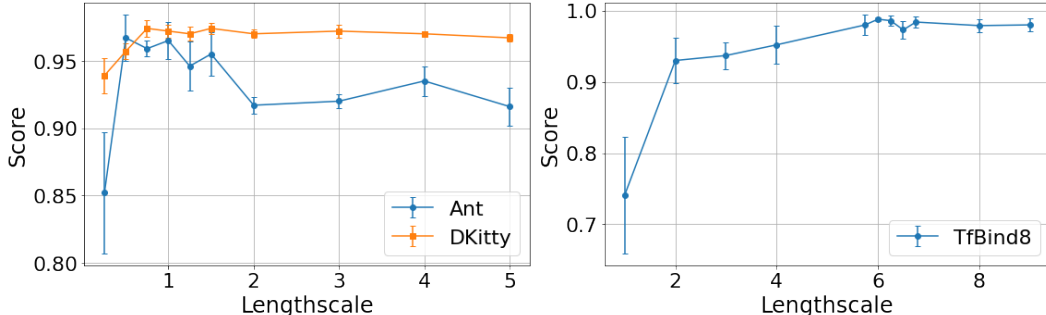


Figure 3: Effect of lengthscale on performance for Ant and DKitty.

GP hyperparameters range size δ and step size η . In the data-generation phase, we uniformly sample the Gaussian process lengthscale and variance from the intervals $[\ell_0 - \delta, \ell_0 + \delta]$ and $[\sigma_0 - \delta, \sigma_0 + \delta]$, respectively (see Line 5 Algorithm 1). Choosing δ is a trade-off: if it is too large, the probabilistic bridge will learn on functions that deviate excessively from the oracle, but if it is too small, we lose the diversity needed for robust generalization. We conducted a sweep over different values of δ ; as shown in Table 18, $\delta = 0.25$ achieves the best performance across both the **Ant** and **TF-Bind-8** tasks. In addition, during this phase we apply M gradient steps with fixed step size η (see Eq.12 and Eq. 13). Our experiments in Table 19 demonstrate that for continuous tasks, setting $\eta = 0.001$ achieves the best score.

Table 18: Performance on **Ant** and **TF-Bind-8** with varying δ .

δ	Ant	TF-Bind-8
0.05	0.953 ± 0.011	0.982 ± 0.005
0.10	0.957 ± 0.014	0.986 ± 0.006
0.25 (ours)	0.965 ± 0.014	0.986 ± 0.007
0.50	0.959 ± 0.013	0.981 ± 0.007
1.00	0.959 ± 0.014	0.989 ± 0.003

Table 20: Performance comparison of different GP kernels on **Ant** and **TF-Bind-8**.

Kernel	Ant	TFBind8
Matern	0.966 ± 0.013	0.848 ± 0.055
RBF	0.965 ± 0.014	0.986 ± 0.007

GP kernel choice. We experimented with the Matern kernel for the GP-based synthetic data generation, as reported in Table 20. The results indicate that the commonly used RBF kernel consistently yields better performance, supporting our decision to use it as the default.

Incorporating explicit uncertainty via acquisition functions. In Gaussian Process literature, incorporating explicit uncertainty via acquisition functions like UCB or LCB is a promising approach for balancing exploration and exploitation. To evaluate this, we conducted a small-scale experiment replacing the GP’s mean function with UCB and LCB scores to generate synthetic data. The results, shown in Table 21, indicate that while UCB and LCB perform reasonably well, they do not outperform our original approach based on the GP’s mean function. We believe this is because uncertainty has already been implicitly captured through a different mechanism, by sampling multiple mean functions from a population of posterior GPs trained on the same offline dataset using different kernel configurations.

C.8 Score and Pseudo-Value Distribution of Generated Samples from GP

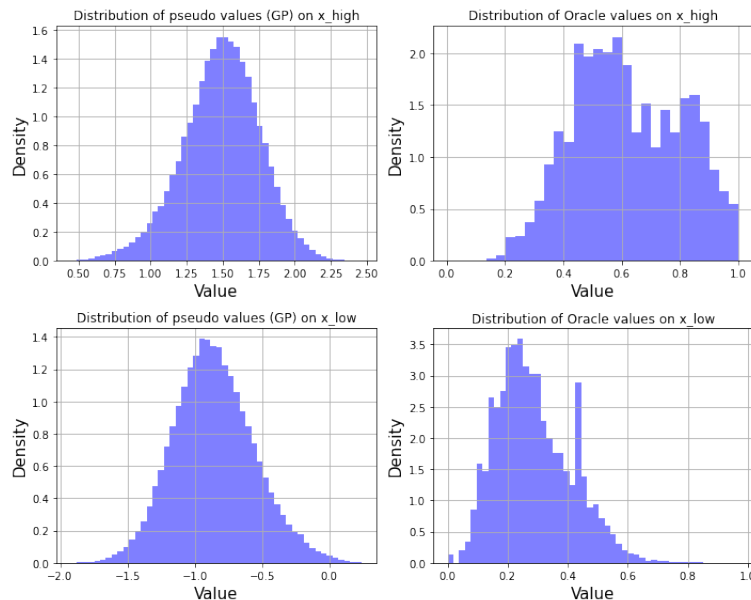


Figure 4: Distribution of pseudo-values (GP) and oracle values on low- and high-value regions.

To further demonstrate the efficiency of Gaussian processes, we conducted an experiment on the **Ant** task using low and high regions produced by 800 GP mean functions. Each function produces 1024 low-value points (\mathbf{X}^- or x_{low}) along with 1024 high-value points (\mathbf{X}^+ or x_{high}). We concatenate all 1024×800 points to form the distribution for the low-value and high-value designs. We then plotted both the oracle value distribution by using the oracle function to evaluate and the pseudo-value distribution (y^- and y^+ predicted by GP). As shown in Figure 4, the low and high regions correspond to two clearly separated distributions. The oracle values in \mathbf{X}^+ are skewed toward higher values, while those in \mathbf{X}^- are skewed toward lower values. This separation facilitates effective training of our probabilistic bridge model as it learns to transform between two distinct distributions.

C.9 Limited Budget Settings

While a budget of $Q = 128$ candidates is a commonly adopted setting, we also conduct experiments under more constrained budgets to evaluate the robustness of our method. The results, shown in Table 22, demonstrate that **ROOT** continues to achieve strong performance even in these highly limited-query scenarios, outperforming existing baselines.

Table 22: Performance of different methods under extreme limited offline data budgets (Q). **ROOT** consistently outperforms baselines on both **Ant** and **TF-Bind-8**.

Q Budget	Method	Ant	TFBind8
16	GA	0.250 ± 0.033	0.938 ± 0.020
	COMs	0.789 ± 0.070	0.917 ± 0.059
	ROOT	0.938 ± 0.022	0.956 ± 0.028
32	GA	0.252 ± 0.036	0.961 ± 0.024
	COMs	0.776 ± 0.033	0.871 ± 0.030
	ROOT	0.942 ± 0.019	0.974 ± 0.020
64	GA	0.281 ± 0.023	0.978 ± 0.020
	COMs	0.834 ± 0.051	0.922 ± 0.036
	ROOT	0.942 ± 0.020	0.974 ± 0.021

C.10 Strong measurement noise setting

Although **ROOT** uses synthetic labels from deterministic GP means, it remains robust to strong measurement noise. This is due to the use of a diverse GP ensemble with varied hyperparameters, which implicitly captures a wide range of uncertainties present in the offline dataset. Sampling from this ensemble produces synthetic data that reflects variability in the objective, helping the bridge model generalize more effectively. To validate this, we ran additional experiments on **TF-Bind-8** with label perturbed by Gaussian noise $\mathbb{N}(0, \epsilon)$. As shown in the Table 23, **ROOT** maintains strong performance and outperforms other baselines across noise levels, demonstrating its resilience to measurement noise.

Table 23: Performance of different methods on **TF-Bind-8** task with label perturbed by measurement noise $\mathbb{N}(0, \epsilon)$.

ϵ	0.01	0.1	0.2
GA	0.967 ± 0.015	0.970 ± 0.006	0.963 ± 0.010
COMs	0.956 ± 0.024	0.925 ± 0.034	0.952 ± 0.013
REINFORCE	0.947 ± 0.030	0.933 ± 0.025	0.930 ± 0.042
ROOT	0.969 ± 0.016	0.971 ± 0.007	0.965 ± 0.014

C.11 High-dimensional continuous task

In the Design-Bench benchmark, the **Hopper** task represents a high-dimensional continuous task with 5,126 input dimensions. Although prior work has noted a highly noisy and inaccurate oracle function for this task, we conducted a small experiment to evaluate **ROOT**'s performance on **Hopper**

as a test of scalability. As shown in the Table 24, **ROOT** outperforms some representative baselines, demonstrating its ability to effectively handle high-dimensional design spaces.

Table 24: Performance of different methods on the Hopper Controller task.

Method	Hopper Controller
GA	-0.068±0.001
MINs	0.267±0.350
Reinforce	-0.009±0.067
ROOT	0.541±0.042

D Broader Impact and Limitation

Broader Impact. This work provides a novel lens for offline black-box optimization by reframing it as a distributional translation problem, potentially inspiring new probabilistic modeling techniques in low-data regimes. The approach opens up new possibilities for data-efficient optimization in applications where function evaluations are expensive or infeasible. These include (but are not limited to) materials discovery, policy design, and automated experimentation. However, caution must be exercised when deploying such methods in safety-critical domains, as reliance on synthetic priors may introduce epistemic uncertainty that requires careful quantification and calibration.

Limitation. One practical consideration is the additional computational overhead introduced by fitting multiple Gaussian processes to construct the synthetic function ensemble. While this step is performed offline and enables better data efficiency during optimization, it may require tuning and parallelization to scale effectively with large input dimensions or limited compute resources.

E Other Practical Setups for Our Probabilistic Bridge Framework

In this paper, we employ the Brownian bridge as our practical probabilistic bridge (see Appendix B.2), which achieves significant performance across our experiments. However, our proposal method is a flexible framework that can be universally adapted to other probabilistic bridges. In this section, we will demonstrate another design: **Ornstein-Uhlenbeck Bridge**.

From our definition of the probabilistic bridge in Section 3.1.1, we can choose ψ_t and $\kappa_{t,k}$ as

$$\psi_t(\mathbf{x}_0, \mathbf{x}_T) = \mathbf{x}_0 \cdot \frac{\sinh(\alpha(T-t))}{\sinh(\alpha T)} + \mathbf{x}_T \cdot \frac{\sinh(\alpha t)}{\sinh(\alpha T)}, \quad (26)$$

$$\kappa_{t,k} = \frac{\sinh(\alpha \cdot \min(t, k)) \cdot \sinh(\alpha \cdot (T - \max(t, k)))}{\alpha \cdot \sinh(\alpha T)}. \quad (27)$$

This choice will result in the formula of the Ornstein-Uhlenbeck bridge [1] with the hyperparameter α . Once this bridge is learned, we can simulate \mathbf{x}_t following the previously derived simulation approach in Eq. 5 which, under the OU instantiation, becomes,

$$\mathbf{x}_t = \mathbf{x}_0 \cdot \frac{\sinh(\alpha(T-t))}{\sinh(\alpha T)} + \mathbf{x}_T \cdot \frac{\sinh(\alpha t)}{\sinh(\alpha T)} + \sqrt{\frac{\sinh(\alpha t) \cdot \sinh(\alpha(T-t))}{\alpha \cdot \sinh(\alpha T)}} \cdot \boldsymbol{\epsilon}_t \quad (28)$$

where $\boldsymbol{\epsilon}_t \sim \mathbb{N}(0, \mathbf{I})$. From the above equation, we can also represent \mathbf{x}_0 in terms of \mathbf{x}_t and \mathbf{x}_T :

$$\mathbf{x}_0 = \left(\mathbf{x}_t - \mathbf{x}_T \cdot \frac{\sinh(\alpha t)}{\sinh(\alpha T)} - \sqrt{\frac{\sinh(\alpha t) \cdot \sinh(\alpha(T-t))}{\alpha \cdot \sinh(\alpha T)}} \cdot \boldsymbol{\epsilon}_t \right) \cdot \frac{\sinh(\alpha T)}{\sinh(\alpha(T-t))}. \quad (29)$$

The transition probability of the localized bridge/flow, i.e., $q(\mathbf{x}_{t-1} \mid \mathbf{x}_t, \mathbf{x}_0, \mathbf{x}_T)$ in Eq. 6, can be derived by using the conditional Gaussian rule which results in the following transition mean,

$$\boldsymbol{\mu}(\mathbf{x}_t, \mathbf{x}_0, \mathbf{x}_T) = \psi_{t-1}(\mathbf{x}_0, \mathbf{x}_T) + \kappa_{t-1, t} \kappa_{t, t}^{-1} (\mathbf{x}_t - \psi_t(\mathbf{x}_0, \mathbf{x}_T)). \quad (30)$$

Table 25: Performance of **ROOT** with different bridge configuration across the benchmark tasks.

Bridges	Ant	D'Kitty	TF-Bind-8	TF-Bind-10
ROOT (BBDM)	0.965 ± 0.014	0.972 ± 0.005	0.986 ± 0.007	0.685 ± 0.053
ROOT (OUDM)	1.940 ± 0.599	0.723 ± 0.001	0.927 ± 0.049	0.675 ± 0.124

Substituting $\mathbf{x}_t = \psi_t(\mathbf{x}_0, \mathbf{x}_T) + \sqrt{\kappa_{t,t}} \cdot \boldsymbol{\epsilon}_t$, the above transition mean can be rewritten as:

$$\boldsymbol{\mu}(\mathbf{x}_t, \mathbf{x}_0, \mathbf{x}_T) = \psi_{t-1}(\mathbf{x}_0, \mathbf{x}_T) + \kappa_{t-1,t} \kappa_{t,t}^{-1/2} \boldsymbol{\epsilon}_t \quad (31)$$

$$\begin{aligned} &= \mathbf{x}_0 \frac{\sinh(\alpha(T-t+1))}{\sinh(\alpha T)} + \mathbf{x}_T \frac{\sinh(\alpha(t-1))}{\sinh(\alpha T)} \\ &+ \boldsymbol{\epsilon}_t \frac{\sinh(\alpha(t-1)) \sinh(\alpha(T-t))}{\sqrt{\alpha \sinh(\alpha T) \sinh(\alpha t) \sinh(\alpha(T-t))}}. \end{aligned} \quad (32)$$

By substituting \mathbf{x}_0 from Eq. 29, we get a closed-form formula for $\boldsymbol{\mu}(\mathbf{x}_t, \mathbf{x}_0, \mathbf{x}_T) = u_t \cdot \mathbf{x}_t + v_t \cdot \mathbf{x}_T + w_t \cdot \boldsymbol{\epsilon}_t$ where the coefficients are computed as

$$u_t = \frac{\sinh(\alpha(T-t+1))}{\sinh(\alpha(T-t))}, \quad v_t = \left[\frac{\sinh(\alpha(t-1))}{\sinh(\alpha T)} - \frac{\sinh(\alpha(T-t+1)) \sinh(\alpha t)}{\sinh(\alpha T) \sinh(\alpha(T-t))} \right], \quad (33)$$

$$w_t = \sqrt{\frac{\sinh(\alpha(T-t))}{\alpha \sinh(\alpha T) \sinh(\alpha t)}} \cdot \left[\sinh(\alpha(t-1)) - \sinh(\alpha t) \cdot \frac{\sinh(\alpha(T-t+1))}{\sinh(\alpha(T-t))} \right]. \quad (34)$$

Next, following prior practice, we again reparameterize the target-agnostic transformation $p_\theta(\mathbf{x}_{t-1} | \mathbf{x}_t, \mathbf{x}_T)$ as a neuralized Gaussian with mean $\boldsymbol{\mu}_\theta(\mathbf{x}_t, \mathbf{x}_0, \mathbf{x}_T) = u_t \cdot \mathbf{x}_t + v_t \cdot \mathbf{x}_T + w_t \cdot \boldsymbol{\epsilon}_\theta(\mathbf{x}_t, \mathbf{x}_T, t)$ and same covariance matrix as the local transition, the (training) ELBO loss in Eq. 8 can be simplified as:

$$\boldsymbol{\theta}_{\text{PB}} = \arg \min_{\boldsymbol{\theta}} \mathbb{E}_{(\mathbf{x}_0, \mathbf{x}_T) \sim D_s, \boldsymbol{\epsilon}_t \sim \mathbb{N}(0, \mathbf{I})} \left\| \boldsymbol{\epsilon}_\theta(\psi_t(\mathbf{x}_0, \mathbf{x}_T) + \kappa_{t,t} \cdot \boldsymbol{\epsilon}_t, \mathbf{x}_T, t) - \boldsymbol{\epsilon}_t \right\|^2. \quad (35)$$

In addition, incorporating the classifier-free guidance techniques leads to:

$$\boldsymbol{\theta}_{\text{PB}} = \arg \min_{\boldsymbol{\theta}} \mathbb{E}_{(\mathbf{x}_0, y_0, \mathbf{x}_T, y_T), \boldsymbol{\epsilon}_t} \left\| \boldsymbol{\epsilon}_\theta(\psi_t(\mathbf{x}_0, \mathbf{x}_T) + \kappa_{t,t} \cdot \boldsymbol{\epsilon}_t, t, \gamma \cdot y + (1 - \gamma) \cdot \emptyset) - \boldsymbol{\epsilon}_t \right\|^2, \quad (36)$$

where $\gamma \sim \text{Ber}(\rho)$. Once the training process is done, we can employ the trained network $\boldsymbol{\epsilon}_\theta$ for our optimization-via-simulation process:

$$\mathbf{x}_{t-1} = u_t \cdot \mathbf{x}_t + v_t \cdot \mathbf{x}_T + w_t \cdot \boldsymbol{\epsilon}_\theta(\mathbf{x}_t, t, y) + \sqrt{\tilde{\kappa}_{t-1}} \cdot \boldsymbol{\epsilon}, \quad (37)$$

where $\tilde{\kappa}_{t-1} = \kappa_{t-1,t-1} - \kappa_{t-1,t} \kappa_{t,t}^{-1} \kappa_{t,t-1}$ and $\boldsymbol{\epsilon} \sim \mathbb{N}(0, \mathbf{I})$.

The performance of the OU-based **ROOT** is compared against the original Brownian-based **ROOT** in Table 25. The results show that the OU-based variant of **ROOT** performs competitively to the original Brownian variant on **TF-Bind-8** and **TF-Bind-10**. On the **Ant** task, the OU-based variant is better while on the **D'Kitty** task, the Brownian variant is better. We leave a more thorough investigation across different variants of **ROOT** with different bridge configuration to future work as such detailed investigation is beyond the scope of our current work.

NeurIPS Paper Checklist

1. Claims

Question: Do the main claims made in the abstract and introduction accurately reflect the paper's contributions and scope?

Answer: [\[Yes\]](#)

Justification: Our contribution can be found in Section 3.

Guidelines:

- The answer NA means that the abstract and introduction do not include the claims made in the paper.
- The abstract and/or introduction should clearly state the claims made, including the contributions made in the paper and important assumptions and limitations. A No or NA answer to this question will not be perceived well by the reviewers.
- The claims made should match theoretical and experimental results, and reflect how much the results can be expected to generalize to other settings.
- It is fine to include aspirational goals as motivation as long as it is clear that these goals are not attained by the paper.

2. Limitations

Question: Does the paper discuss the limitations of the work performed by the authors?

Answer: [\[Yes\]](#)

Justification: We discuss our limitations in Appendix D.

Guidelines:

- The answer NA means that the paper has no limitation while the answer No means that the paper has limitations, but those are not discussed in the paper.
- The authors are encouraged to create a separate "Limitations" section in their paper.
- The paper should point out any strong assumptions and how robust the results are to violations of these assumptions (e.g., independence assumptions, noiseless settings, model well-specification, asymptotic approximations only holding locally). The authors should reflect on how these assumptions might be violated in practice and what the implications would be.
- The authors should reflect on the scope of the claims made, e.g., if the approach was only tested on a few datasets or with a few runs. In general, empirical results often depend on implicit assumptions, which should be articulated.
- The authors should reflect on the factors that influence the performance of the approach. For example, a facial recognition algorithm may perform poorly when image resolution is low or images are taken in low lighting. Or a speech-to-text system might not be used reliably to provide closed captions for online lectures because it fails to handle technical jargon.
- The authors should discuss the computational efficiency of the proposed algorithms and how they scale with dataset size.
- If applicable, the authors should discuss possible limitations of their approach to address problems of privacy and fairness.
- While the authors might fear that complete honesty about limitations might be used by reviewers as grounds for rejection, a worse outcome might be that reviewers discover limitations that aren't acknowledged in the paper. The authors should use their best judgment and recognize that individual actions in favor of transparency play an important role in developing norms that preserve the integrity of the community. Reviewers will be specifically instructed to not penalize honesty concerning limitations.

3. Theory assumptions and proofs

Question: For each theoretical result, does the paper provide the full set of assumptions and a complete (and correct) proof?

Answer: [\[NA\]](#)

Justification: We do not provide theoretical results. Our main contribution is translating the offline optimization problem to a probabilistic bridge framework.

Guidelines:

- The answer NA means that the paper does not include theoretical results.
- All the theorems, formulas, and proofs in the paper should be numbered and cross-referenced.
- All assumptions should be clearly stated or referenced in the statement of any theorems.
- The proofs can either appear in the main paper or the supplemental material, but if they appear in the supplemental material, the authors are encouraged to provide a short proof sketch to provide intuition.
- Inversely, any informal proof provided in the core of the paper should be complemented by formal proofs provided in appendix or supplemental material.
- Theorems and Lemmas that the proof relies upon should be properly referenced.

4. Experimental result reproducibility

Question: Does the paper fully disclose all the information needed to reproduce the main experimental results of the paper to the extent that it affects the main claims and/or conclusions of the paper (regardless of whether the code and data are provided or not)?

Answer: [\[Yes\]](#)

Justification: All information regarding our experiments are disclosed in Section 4 and in the Appendix.

Guidelines:

- The answer NA means that the paper does not include experiments.
- If the paper includes experiments, a No answer to this question will not be perceived well by the reviewers: Making the paper reproducible is important, regardless of whether the code and data are provided or not.
- If the contribution is a dataset and/or model, the authors should describe the steps taken to make their results reproducible or verifiable.
- Depending on the contribution, reproducibility can be accomplished in various ways. For example, if the contribution is a novel architecture, describing the architecture fully might suffice, or if the contribution is a specific model and empirical evaluation, it may be necessary to either make it possible for others to replicate the model with the same dataset, or provide access to the model. In general, releasing code and data is often one good way to accomplish this, but reproducibility can also be provided via detailed instructions for how to replicate the results, access to a hosted model (e.g., in the case of a large language model), releasing of a model checkpoint, or other means that are appropriate to the research performed.
- While NeurIPS does not require releasing code, the conference does require all submissions to provide some reasonable avenue for reproducibility, which may depend on the nature of the contribution. For example
 - (a) If the contribution is primarily a new algorithm, the paper should make it clear how to reproduce that algorithm.
 - (b) If the contribution is primarily a new model architecture, the paper should describe the architecture clearly and fully.
 - (c) If the contribution is a new model (e.g., a large language model), then there should either be a way to access this model for reproducing the results or a way to reproduce the model (e.g., with an open-source dataset or instructions for how to construct the dataset).
 - (d) We recognize that reproducibility may be tricky in some cases, in which case authors are welcome to describe the particular way they provide for reproducibility. In the case of closed-source models, it may be that access to the model is limited in some way (e.g., to registered users), but it should be possible for other researchers to have some path to reproducing or verifying the results.

5. Open access to data and code

Question: Does the paper provide open access to the data and code, with sufficient instructions to faithfully reproduce the main experimental results, as described in supplemental material?

Answer: [\[Yes\]](#)

Justification: Our code is available at an anonymous repository (see Appendix B), and all experiments are run on publicly available datasets.

Guidelines:

- The answer NA means that paper does not include experiments requiring code.
- Please see the NeurIPS code and data submission guidelines (<https://nips.cc/public/guides/CodeSubmissionPolicy>) for more details.
- While we encourage the release of code and data, we understand that this might not be possible, so “No” is an acceptable answer. Papers cannot be rejected simply for not including code, unless this is central to the contribution (e.g., for a new open-source benchmark).
- The instructions should contain the exact command and environment needed to run to reproduce the results. See the NeurIPS code and data submission guidelines (<https://nips.cc/public/guides/CodeSubmissionPolicy>) for more details.
- The authors should provide instructions on data access and preparation, including how to access the raw data, preprocessed data, intermediate data, and generated data, etc.
- The authors should provide scripts to reproduce all experimental results for the new proposed method and baselines. If only a subset of experiments are reproducible, they should state which ones are omitted from the script and why.
- At submission time, to preserve anonymity, the authors should release anonymized versions (if applicable).
- Providing as much information as possible in supplemental material (appended to the paper) is recommended, but including URLs to data and code is permitted.

6. Experimental setting/details

Question: Does the paper specify all the training and test details (e.g., data splits, hyper-parameters, how they were chosen, type of optimizer, etc.) necessary to understand the results?

Answer: [\[Yes\]](#)

Justification: We included such details in the Appendix B.

Guidelines:

- The answer NA means that the paper does not include experiments.
- The experimental setting should be presented in the core of the paper to a level of detail that is necessary to appreciate the results and make sense of them.
- The full details can be provided either with the code, in appendix, or as supplemental material.

7. Experiment statistical significance

Question: Does the paper report error bars suitably and correctly defined or other appropriate information about the statistical significance of the experiments?

Answer: [\[Yes\]](#)

Justification: We do report error bars in our experiments.

Guidelines:

- The answer NA means that the paper does not include experiments.
- The authors should answer “Yes” if the results are accompanied by error bars, confidence intervals, or statistical significance tests, at least for the experiments that support the main claims of the paper.
- The factors of variability that the error bars are capturing should be clearly stated (for example, train/test split, initialization, random drawing of some parameter, or overall run with given experimental conditions).

- The method for calculating the error bars should be explained (closed form formula, call to a library function, bootstrap, etc.)
- The assumptions made should be given (e.g., Normally distributed errors).
- It should be clear whether the error bar is the standard deviation or the standard error of the mean.
- It is OK to report 1-sigma error bars, but one should state it. The authors should preferably report a 2-sigma error bar than state that they have a 96% CI, if the hypothesis of Normality of errors is not verified.
- For asymmetric distributions, the authors should be careful not to show in tables or figures symmetric error bars that would yield results that are out of range (e.g. negative error rates).
- If error bars are reported in tables or plots, The authors should explain in the text how they were calculated and reference the corresponding figures or tables in the text.

8. Experiments compute resources

Question: For each experiment, does the paper provide sufficient information on the computer resources (type of compute workers, memory, time of execution) needed to reproduce the experiments?

Answer: [\[Yes\]](#)

Justification: The information about our computation resources is detailed C.1.

Guidelines:

- The answer NA means that the paper does not include experiments.
- The paper should indicate the type of compute workers CPU or GPU, internal cluster, or cloud provider, including relevant memory and storage.
- The paper should provide the amount of compute required for each of the individual experimental runs as well as estimate the total compute.
- The paper should disclose whether the full research project required more compute than the experiments reported in the paper (e.g., preliminary or failed experiments that didn't make it into the paper).

9. Code of ethics

Question: Does the research conducted in the paper conform, in every respect, with the NeurIPS Code of Ethics <https://neurips.cc/public/EthicsGuidelines>?

Answer: [\[Yes\]](#)

Justification: We have read the NeurIPS Code of Ethics and believe that our work does not violate any of its principles.

Guidelines:

- The answer NA means that the authors have not reviewed the NeurIPS Code of Ethics.
- If the authors answer No, they should explain the special circumstances that require a deviation from the Code of Ethics.
- The authors should make sure to preserve anonymity (e.g., if there is a special consideration due to laws or regulations in their jurisdiction).

10. Broader impacts

Question: Does the paper discuss both potential positive societal impacts and negative societal impacts of the work performed?

Answer: [\[Yes\]](#)

Justification: We did discussed it in Appendix D

Guidelines:

- The answer NA means that there is no societal impact of the work performed.
- If the authors answer NA or No, they should explain why their work has no societal impact or why the paper does not address societal impact.

- Examples of negative societal impacts include potential malicious or unintended uses (e.g., disinformation, generating fake profiles, surveillance), fairness considerations (e.g., deployment of technologies that could make decisions that unfairly impact specific groups), privacy considerations, and security considerations.
- The conference expects that many papers will be foundational research and not tied to particular applications, let alone deployments. However, if there is a direct path to any negative applications, the authors should point it out. For example, it is legitimate to point out that an improvement in the quality of generative models could be used to generate deepfakes for disinformation. On the other hand, it is not needed to point out that a generic algorithm for optimizing neural networks could enable people to train models that generate Deepfakes faster.
- The authors should consider possible harms that could arise when the technology is being used as intended and functioning correctly, harms that could arise when the technology is being used as intended but gives incorrect results, and harms following from (intentional or unintentional) misuse of the technology.
- If there are negative societal impacts, the authors could also discuss possible mitigation strategies (e.g., gated release of models, providing defenses in addition to attacks, mechanisms for monitoring misuse, mechanisms to monitor how a system learns from feedback over time, improving the efficiency and accessibility of ML).

11. Safeguards

Question: Does the paper describe safeguards that have been put in place for responsible release of data or models that have a high risk for misuse (e.g., pretrained language models, image generators, or scraped datasets)?

Answer: [NA]

Justification: Our work does not create any new datasets or pre-trained models. We solely use existing, publicly available datasets.

Guidelines:

- The answer NA means that the paper poses no such risks.
- Released models that have a high risk for misuse or dual-use should be released with necessary safeguards to allow for controlled use of the model, for example by requiring that users adhere to usage guidelines or restrictions to access the model or implementing safety filters.
- Datasets that have been scraped from the Internet could pose safety risks. The authors should describe how they avoided releasing unsafe images.
- We recognize that providing effective safeguards is challenging, and many papers do not require this, but we encourage authors to take this into account and make a best faith effort.

12. Licenses for existing assets

Question: Are the creators or original owners of assets (e.g., code, data, models), used in the paper, properly credited and are the license and terms of use explicitly mentioned and properly respected?

Answer: [Yes]

Justification: All datasets used in our experiments are properly cited.

Guidelines:

- The answer NA means that the paper does not use existing assets.
- The authors should cite the original paper that produced the code package or dataset.
- The authors should state which version of the asset is used and, if possible, include a URL.
- The name of the license (e.g., CC-BY 4.0) should be included for each asset.
- For scraped data from a particular source (e.g., website), the copyright and terms of service of that source should be provided.

- If assets are released, the license, copyright information, and terms of use in the package should be provided. For popular datasets, paperswithcode.com/datasets has curated licenses for some datasets. Their licensing guide can help determine the license of a dataset.
- For existing datasets that are re-packaged, both the original license and the license of the derived asset (if it has changed) should be provided.
- If this information is not available online, the authors are encouraged to reach out to the asset's creators.

13. New assets

Question: Are new assets introduced in the paper well documented and is the documentation provided alongside the assets?

Answer: [NA]

Justification: No new assets are released as part of our work.

Guidelines:

- The answer NA means that the paper does not release new assets.
- Researchers should communicate the details of the dataset/code/model as part of their submissions via structured templates. This includes details about training, license, limitations, etc.
- The paper should discuss whether and how consent was obtained from people whose asset is used.
- At submission time, remember to anonymize your assets (if applicable). You can either create an anonymized URL or include an anonymized zip file.

14. Crowdsourcing and research with human subjects

Question: For crowdsourcing experiments and research with human subjects, does the paper include the full text of instructions given to participants and screenshots, if applicable, as well as details about compensation (if any)?

Answer: [NA]

Justification: Our work does not involve crowdsourcing nor research with human subjects.

Guidelines:

- The answer NA means that the paper does not involve crowdsourcing nor research with human subjects.
- Including this information in the supplemental material is fine, but if the main contribution of the paper involves human subjects, then as much detail as possible should be included in the main paper.
- According to the NeurIPS Code of Ethics, workers involved in data collection, curation, or other labor should be paid at least the minimum wage in the country of the data collector.

15. Institutional review board (IRB) approvals or equivalent for research with human subjects

Question: Does the paper describe potential risks incurred by study participants, whether such risks were disclosed to the subjects, and whether Institutional Review Board (IRB) approvals (or an equivalent approval/review based on the requirements of your country or institution) were obtained?

Answer: [NA]

Justification: Our work does not involve human subjects or crowdsourcing

Guidelines:

- The answer NA means that the paper does not involve crowdsourcing nor research with human subjects.
- Depending on the country in which research is conducted, IRB approval (or equivalent) may be required for any human subjects research. If you obtained IRB approval, you should clearly state this in the paper.

- We recognize that the procedures for this may vary significantly between institutions and locations, and we expect authors to adhere to the NeurIPS Code of Ethics and the guidelines for their institution.
- For initial submissions, do not include any information that would break anonymity (if applicable), such as the institution conducting the review.

16. Declaration of LLM usage

Question: Does the paper describe the usage of LLMs if it is an important, original, or non-standard component of the core methods in this research? Note that if the LLM is used only for writing, editing, or formatting purposes and does not impact the core methodology, scientific rigorousness, or originality of the research, declaration is not required.

Answer: [NA]

Justification: We did not use LLMs assistance at any point in our core methods.

Guidelines:

- The answer NA means that the core method development in this research does not involve LLMs as any important, original, or non-standard components.
- Please refer to our LLM policy (<https://neurips.cc/Conferences/2025/LLM>) for what should or should not be described.